H3K27me3-modulated Hofbauer cell BMP2 signalling enhancement compensates for shallow trophoblast invasion in preeclampsia

Jianye Deng,[a,b,j] Hong-Jin Zhao,[c,d,j] Ying Zhong,[e,j] Cuiping Hu,[a] Jinlai Meng,[f] Chunling Wang,[g] Xiangxin Lan,[a] Xiyao Wang,[a] Zi-Jiang Chen,[a] Junhao Yan,[a,***] Wei Wang,[h,**] and Yan Li[a,b,i,*]

[a]Center for Reproductive Medicine, Shandong University, Jinan, Shandong, 250012, China
[b]Medical Integration and Practice Center, Shandong University, Jinan, Shandong, 250012, China
[c]Department of Cardiology, Shandong Provincial Hospital Affiliated to Shandong First Medical University, Jinan, Shandong, 250021, China
[d]Department of Cardiology, Shandong Provincial Hospital, Shandong University, Jinan, Shandong, 250021, China
[e]Cardiovascular Research Center of the General Medical Services, Massachusetts General Hospital, Boston, MA, 02129, USA
[f]Department of Obstetrics and Gynaecology, Shandong Provincial Hospital, Shandong University, Jinan, Shandong, 250021, China
[g]Department of Anesthesiology, Qilu Hospital of Shandong University, Jinan, Shandong, 250012, China
[h]Division of Neonatology, Department of Pediatrics, Massachusetts General Hospital, Boston, MA 02115, USA

eBioMedicine
2023;93: 104664
Published Online xxx
https://doi.org/10.1016/j.ebiom.2023.104664

Summary

Background Preeclampsia (PE) is a common hypertensive pregnancy disorder associated with shallow trophoblast invasion. Although bone morphogenetic protein 2 (BMP2) has been shown to promote trophoblast invasion *in vitro*, its cellular origin and molecular regulation in placenta, as well as its potential role in PE, has yet to be established. Additionally, whether BMP2 and/or its downstream molecules could serve as potential diagnostic or therapeutic targets for PE has not been explored.

Methods Placentas and sera from PE and healthy pregnant women were subjected to multi-omics analyses, immunoblots, qPCR, and ELISA assays. Immortalized trophoblast cells, primary cultures of human trophoblasts, and first-trimester villous explants were used for *in vitro* experiments. Adenovirus expressing sFlt-1 (Ad Flt1)-induced PE rat model was used for *in vivo* studies.

Findings We find globally decreased H3K27me3 modifications and increased BMP2 signalling in preeclamptic placentas, which is negatively correlated with clinical manifestations. BMP2 is derived from Hofbauer cells and epigenetically regulated by H3K27me3 modification. BMP2 promotes trophoblast invasion and vascular mimicry by upregulating BMP6 via BMPR1A-SMAD2/3-SMAD4 signalling. BMP2 supplementation alleviates high blood pressure and fetal growth restriction phenotypes in Ad Flt1-induced rat PE model.

Interpretation Our findings demonstrate that epigenetically regulated Hofbauer cell-derived BMP2 signalling enhancement in late gestation could serve as a compensatory response for shallow trophoblast invasion in PE, suggesting opportunities for diagnostic marker and therapeutic target applications in PE clinical management.

Funding National Key Research and Development Program of China (2022YFC2702400), National Natural Science Foundation of China (82101784, 82171648, 31988101), and Natural Science Foundation of Shandong Province (ZR2020QH051, ZR2020MH039).

Keywords: BMP2; BMP6; H3K27me3; Hofbauer cell; Trophoblast; Preeclampsia

*Corresponding author. Shandong University, Jinan, China.
**Corresponding author. Massachusetts General Hospital, Boston, MA, USA.
***Corresponding author. Shandong University, Jinan, China.
E-mail addresses: yanli.sdu@gmail.com (Y. Li), wwang@mgh.harvard.edu (W. Wang), yyy306@126.com (J. Yan).
[i]Lead contact.
[j]These authors contributed equally.
Disclosure summary: The authors have nothing to disclose.

Research in context

Evidence before this study

Shallow trophoblast invasion causes improper maternal spiral artery remodeling and poor placentation, which eventually leads to PE, a common human-specific hypertensive pregnancy disorder. Although BMP2 has been shown to promote trophoblast invasion *in vitro*, its potential role in PE has yet to be established. Besides, the cellular origin and molecular regulation of BMP2 in placenta remain unknown.

Added value of this study

Our study shows that H3K27me3 modified BMP2 signalling increases in preeclamptic placentas at delivery but is negatively correlated with PE clinical manifestations. BMP2 is derived from Hofbauer cells in placenta and promotes trophoblast invasion and vascular mimicry by upregulating BMP6 via BMPR1A-SMAD2/3-SMAD4 signalling. In addition, BMP2 supplementation at middle pregnancy stage ameliorates high blood pressure and fetal growth restriction in rat PE model.

Implications of all the available evidence

This study increases our knowledge of the cellular origin and molecular regulation of BMP2 in placenta and highlights a self-compensatory role of BMP2 signalling in PE. These findings indicate that BMP2 and its downstream molecules may serve as diagnostic markers and therapeutic targets for PE clinical management.

Introduction

Preeclampsia (PE) is characterized by the *de novo* development of concurrent high blood pressure (≥140/90 mmHg) and proteinuria (≥300 mg/L per 24 h) after 20 weeks of gestation. As a complex, heterogeneous syndrome complicating 2%–8% of human pregnancies, PE remains a leading cause of maternal and perinatal mortality and morbidity worldwide.[1,2] It is also notable that PE predisposes both mothers and offspring to future cardiovascular diseases in the long term,[3,4] underlining the medical utility of elucidating the pathophysiological mechanisms of PE and developing effective interventions for its clinical management.

Considerable PE research has revealed that shallow trophoblast invasion leads to subsequent improper maternal spiral artery remodeling and poor placentation,[5,6] specifically by promoting the release of anti-angiogenic factors in maternal circulation that result in systematic endothelial dysfunction and corresponding clinical manifestations.[3,7] Trophoblast invasion during early human placentation refers to the process by which a subset of trophoblasts that originate at the tip of anchoring villi (termed as extravillous trophoblast (EVT) cells) invade the maternal decidua and remodel the uterine spiral arteries upon acquiring invasive and vascular mimicry abilities.[8] Transforming growth factor-β (TGF-β) superfamily member proteins, along with a plethora of regulating factors, exert divergent functions in regulating the trophoblast invasion process.[8] The dysregulation of several TGF-β superfamily proteins, including TGF-β1-3, Nodal, and activin A, has also been observed in PE patients, supporting that TGF-β proteins have the potential to serve as candidate diagnostic and therapeutic targets for PE.[8] However, whether other TGF-β superfamily proteins are dysregulated in PE patients and what roles such dysregulated proteins may play in PE pathogenesis remain to be determined.

Bone morphogenetic proteins (BMPs) are highly conserved members of the TGF-β superfamily; these secreted proteins have known functions in development, angiogenesis, and reproduction.[9–11] TGF-β superfamily members exert their biological effects by activating type I and type II transmembrane serine/threonine kinase receptors to trigger downstream canonical (SMAD) or non-canonical (non-SMAD) signal transduction. TGF-β superfamily members first bind to extracellular domain of type II receptor, then a type I receptor is recruited. After that, downstream signal transduction molecules are phosphorylated by the type I receptor. For BMPs, SMAD1/5/9 have been regarded as the canonical downstream mediators; however, non-canonical SMAD2/3 activation for mediation of BMP2 signalling has also been identified.[12] Among the seven type I receptors (activin receptor-like kinases 1 to 7, ALK1-7) for TGF-β superfamily proteins in humans, ALK1 (ACVRL1), ALK2 (ACVR1), ALK3 (BMPR1A) and ALK6 (BMPR1B) have been demonstrated as type I receptors for BMPs.[9] There are three known type II receptors for BMPs in mammals: BMP type II receptor (BMPR2), activin type II receptor (ACVR2), and activin type IIB receptor (ACVR2B). Although BMPs, including BMP2, BMP4, BMP6, and BMP10, are essential for trophoblast differentiation of human embryonic stem cells during early embryonic development,[13–15] only BMP2 has to date been identified as a pro-invasive factor that can regulate the invasive behavior of human trophoblasts *in vitro*.[12] However, the cellular origin of BMP2 in placenta, and whether dysregulated placental BMP2 signalling impacts PE pathogenesis, have yet to be established.

Roles for epigenetic modifications in regulating placental development have been gradually revealed.[16] Studies examining the roles of epigenetic regulation in the etiology of PE are still limited; however, it has been

suggested that the identification of epigenetic-based targets related to PE could help identify potential biomarkers for the onset of PE, as well as for classifying PE according to severity.[17] Among the best-illustrated epigenetic effects of histone modifications on placental development,[18] trimethylation of lysine 27 of histone H3 (H3K27me3), a marker of tightly packaged heterochromatin and related to gene repression,[19] is known to participate in regulating the expression of *MMP2/9*, which are associated with trophoblast invasiveness.[20] H3K27me3 is catalyzed by enhancer of zeste homolog 2 (EZH2), which is the catalytic subunit (with histone methyltransferase activity) of polycomb repressive complex 2 (PRC2).[21] A previous study reported that *BMP2* can be regulated by H3K27me3 modification in mouse embryonic fibroblast[22]; however, it remains unclear whether H3K27me3 contributes to dysregulated placental BMP2 signalling during PE development.

Here, using a combination of multi-omics analyses of patients' placentas and sera, *in vitro* assays with immortalized human EVT cells, primary human Hofbauer cells, and first-trimester villous explants, as well as an Ad Flt1-induced rat PE model, we have demonstrated that H3K27me3-modulated BMP2 signalling enhancement in human Hofbauer cells compensates for shallow trophoblast invasion in preeclamptic placentas, providing potential molecular targets for PE clinical management.

Methods

Patients and sample collection

Placental tissues from women with healthy pregnancy (HP) or with clinical diagnosis of PE were collected within 5 min after C-section deliveries (27–42 weeks gestation) at the Department of Obstetrics, Shandong Provincial Hospital. Briefly, the central maternal side of the placenta was dissected, washed with cold sterile saline, aliquoted, and quickly frozen with liquid nitrogen. Corresponding maternal blood samples were collected on the morning of delivery day. Sera were immediately isolated, sub-bottled, and stored at –80 °C until being assayed using Human BMP6 and BMP2 ELISA kit (LSBio, LS-F4538; R&D, DBP200). The detailed clinical characteristics of the 42 women with HP and the 27 women with PE are summarized in Table 1. Human first-trimester chorionic villi from HP that underwent elective terminations (6–8 weeks of gestation) were collected at the Department of Obstetrics, Qilu Hospital, and processed for villous explant culture within 1 h.

Diagnostic criteria

The American College of Obstetrics and Gynecology criteria were used to identify PE patients.[23,24] PE was defined as hypertension that appeared after 20 weeks of gestation with proteinuria (≥0.3 mg urinary protein per 24 h). Hypertension was defined as systolic blood pressure (SBP) ≥ 140 mm hydrargyrum (Hg) or diastolic blood pressure (DBP) ≥ 90 mm Hg in two successive measurements 4–6 h apart. Healthy samples were obtained from women without pregnancy complications who chose to receive C-sections for psychosocial reasons. Patients with evidence of inflammation were excluded on the basis of the following criteria: maternal fever >37.3 °C, uterine tenderness, fetal tachycardia (fetal heart rate >160 beats per min) and/or (placental) histological criteria compatible with inflammation. Other exclusion criteria for the PE and HP groups included pre-existing medical conditions such as a maternal history of hypertension and/or renal disease, cardiovascular disease, diabetes, smoking, alcoholism, chemical dependency, premature rupture of the membranes, and fetal anomaly. Preterm placenta refers to the placenta obtained from preterm delivery which occurs before 37 weeks of gestation. Full term placenta refers to the placenta obtained from full term delivery which occurs after 37 weeks of gestation.

Animal study

9-week-old Sprague–Dawley rats (200–220 g) were purchased from Beijing Vital River Laboratory Animal Technology Co., Ltd (RRID:RGD_734476). All animals were fed a standard laboratory diet and maintained within a 12:12-h light/dark cycle. Gestational day 1 (G1) was determined upon the presence of vaginal plug the following morning. Pregnant rats were randomly divided into 4 groups: Ad Fc + PBS (n = 3), Ad Fc + BMP2 (n = 3), Ad Flt1 + PBS (n = 3), and Ad Flt1 + BMP2 (n = 3). Adenoviruses expressing sFlt-1 or control Fc were purchased from Genechem (Shanghai, China). The detailed construction of the adenoviral plasmid has been described previously.[25,26] 1×10^9 PFU of adenovirus was injected into the tail vein on G8 (early second trimester). Recombinant BMP2 protein (10 μg/kg/day) (R&D, 355-BM-010) or vehicle was injected into the tail vein on G10 to G13. SBP and mean blood pressure (MBP) on G7, G10, G13, G16 and G19 were recorded via tail-cuff plethysmography (MRBP system, IITC Life Science, Woodland Hills, CA, USA). Rats were habituated to the experimental environment by training using a restrainer with a tail cuff for 30 min for two consecutive days. Before the measurement, the rats were restrained and placed in the chamber at a constant temperature of 32 °C for 15–20 min to calm them down, and then 5 consecutive measurements were performed with an interval of 1 min. The rats had to rest for 5 min before the next measurement. DBP values were calculated with the equation DBP = (3MBP-SBP)/2. For micro-computed tomographic imaging (micro-CT), rats were scanned under isoflurane (Ruiwode Lifescience, Shenzhen, China) anesthesia using a small animal Quantum GX2 microCT (PerkinElmer, Waltham, MA, USA) on G19. Scanning parameters were as follows: copper and aluminium filter 0.06 mm + 0.5 mm,

Characteristics	qPCR & ELISA			Bulk RNA sequencing		
	Preeclampsia (N = 27)	Healthy pregnancy (N = 42)	p value	Preeclampsia (N = 7)	Healthy Pregnancy (N = 7)	p value
Age (yr)- Mean ± SD	35.4 ± 4.5	33.4 ± 3.8	0.105	36.0 ± 6.2	32.9 ± 2.8	0.243
Height (cm)- Median (P25, P75) or Mean ± SD[a]	162 (158, 167)	162 (158, 165)	0.637	159 ± 6.9	163 ± 5.1	0.293
Weight (kg)- Median (P25, P75) or Mean ± SD[a]	84 (78, 95)	75.8 (68.75, 84)	0.005	75.1 ± 6.9	72.9 ± 8.8	0.604
BMI (kg/m^2)- Mean ± SD	33.13 ± 5.15	29.34 ± 3.57	0.003	29.63 ± 2.22	27.44 ± 2.61	0.117
SBP (mmHg)- Median (P25, P75)	163 (160, 180)	109 (102.75, 119)	<0.001	152 (150, 160)	121 (115, 125)	<0.001
DBP (mmHg)- Median (P25, P75)	110 (100, 120)	72 (68, 78)	<0.001	100 (89,100)	78 (72, 80)	<0.001
Primigravida- no.	4	9	0.493	0	3	0.192
Parity (times)- Median (P25, P75)	1 (1, 1)	1 (0, 1)	0.121	1 (0, 1)	1 (0, 2)	0.493
Gestational age at delivery (week)- Median (P25, P75)	31.6 (28.7, 37.1)	38.6 (38.3, 39.0)	<0.001	33.1 (31.3,36.6)	37.6(37.4,38.2)	0.004
Infant's birth weight (g)- Median (P25, P75)	1480 (900, 2980)	3335 (3018, 3590)	<0.001	1600 (1150, 3150)	3500 (3300, 3750)	0.001
Male infant- no.	12	22	0.520	5	4	0.152
Delivery at <37 weeks- no.	20	0	<0.001	6	0	0.005
SGA-no.	17	1	<0.001	3	0	0.192
Singleton pregnancy- no.	27	42	–	7	7	–

BMI: body mass index; SBP: systolic blood pressure; DBP: diastolic blood pressure; SGA: small for gestational age (<10th percentile). [a]For normally distributed data, the mean ± SD is presented. Otherwise, the median (P25, P75) is presented. Normality was assessed by Kolmogorov–Smirnov tests.

Table 1: **Characteristics of healthy and preeclamptic pregnancies for RNA-seq, qPCR, and ELISA.**

respectively, 1° rotation step over 360°, source voltage 90 kV, source current 88 μA, image isotropic pixel size 288 μm. Scan mode at Standard, scanning time 2 min. PerkinElmer Quantum GX2 4.0 software was used for image acquisition and reconstruction. Serum and urine on G7, G13 and G19 were collected and measured by sFlt-1 ELISA kit (Proteintech, KE10069), albumin ELISA kit (Abcam, ab108789), and creatinine assay kit (Abcam, ab65340), respectively. Kidney was collected on G19 for histology. Placentas were collected on G19 for histology and measurement of weight and *Bmp2* mRNA level by qPCR. The weights of maternal rats and fetal rats were also measured on indicated days.

Reagents, antibodies, software and algorithms

All reagents, antibodies, software and algorithms were listed in Supplementary Table S1 with a catalogue number and Research Resource Identifier. Commercial antibodies were validated and relevant documentation are shown in the Supplemental Data (Reagent and Cell Line Identification File).

Bulk RNA sequencing and data processing

Total RNA from placental tissues or cells was extracted using TRIzol reagent (Thermofisher, 15596018). mRNA purification, fragmentation, cDNA synthesis, and library construction were performed by Novogene Corporation (Beijing, China). The library preparations were sequenced on the Illumina Novaseq 6000 platform. Raw reads in fastq format were first processed using in-house Perl scripts. Clean reads were obtained by removing reads containing adapters, N bases and low-quality reads from raw data. An index of reference genome was built, and paired-end clean reads were aligned to the human hg38 reference genome using Hisat2 v2.0.5. featureCounts v1.5.0-p3 was used to count the read numbers mapped to each gene. Differential expression analysis and principal component analysis (PCA) were performed using the DESeq2 R package (1.30.0). Gene set enrichment analysis (GSEA) was performed using the GSEA Molecular Signatures Database with the fgsea R package (1.16.0). Heatmaps were generated using the ComplexHeatmap R package (2.6.2). Venn diagrams were made using the VennDiagram R package (1.6.20). Dot plots and waterfall plots were made using the ggplot2 R package (3.3.3).

Chromatin immunoprecipitation sequencing (ChIP-seq) and data processing

The human placental tissues were cut into small pieces and ChIP was performed as previously described using anti-trimethyl-histone H3 (Lys27) (C36B11) rabbit mAb (1:50, Cell Signaling Technology, 9733).[27] ChIP-seq libraries were constructed by Novogene Corporation (Beijing, China) using the purified DNA. Paired-end sequencing of the samples was performed on the Illumina NovaSeq6000 platform. FastQC was used to perform basic statistics on the quality of raw reads. Then, these read sequences were pre-processed through Trimmomatic software: remove adapters and low-quality reads with a mean quality value less than 20 or containing more than 15% N bases; drop reads below 18 bases long after trimming. The remaining reads that passed all the filtering steps were counted as clean reads, and FastQC was used to perform basic statistics on the quality of the clean reads. An index of the human hg38 reference genome was built and clean reads were aligned to the reference genome using BWA mem v 0.7.12. The MACS2 v2.1.0 peak finding algorithm was used to identify regions of IP enrichment (over

background). A q value threshold of enrichment of 0.05 was used for all datasets. The ChIPseeker R package (1.26.0) was used to annotate peaks. The DiffBind R package (3.0.11) was used to perform differential peak analysis. The EnrichedHeatmap R package (1.20.0) was used to make the heatmap. The ChIPpeakAnno R package (4.0.4) was used to make the aggregate plots of the ChIP signals. The karyoploteR R package (1.16.0) was used to create the karyoplots showing H3K27me3 ChIP-seq tracks.

Single-cell RNA sequencing data analysis

Two scRNA-seq datasets of placentas from 5 HP and 5 PE patients[28,29] were re-analyzed by the Seurat R package (4.0.5) in our study. The clinical characteristics of the donors with HP and PE are summarized in Supplementary Table S3. Cells were first filtered with the following criteria: gene number >500 and mitochondrial gene percentage <20% in droplet-based data; gene number >1000 and mitochondrial gene percentage <20% in Smart-seq2 data. To remove batch effects due to background contamination of cell free RNA, a set of genes that had a tendency to be expressed in ambient RNA (PAEP, HBG1, HBA1, HBA2, HBM, AHSP and HBG2) were also removed. After filtering, a filtered gene-barcode matrix of all samples was integrated to remove batch effects across different donors. In particular, 2000 shared highly variable genes were identified using Seurat's 'SelectIntegrationFeatures()' function. Integration anchors were identified based on these genes using canonical correlation analysis with 90 dimensions by the 'FindTransferAnchors()' function. The data were then integrated using 'IntegrateData()' and scaled using 'ScaleData()'. PCA and uniform manifold approximation and projection (UMAP) dimension reduction with 40 principal components were performed. A nearest–neighbor graph using the 40 dimensions of the PCA reduction was calculated using 'FindNeighbors()', followed by clustering using 'FindClusters()' with a resolution of 0.93. Conserved markers for each cluster were identified using 'FindAllMarkers()'. Cells were re-annotated according to the markers identified in original publications. To visualize *BMP2* and *BMPR1A* expression among different cell types in the placenta, 'FeaturePlot()' and 'VlnPlot()' were used. GSEA was performed using the GSEA Molecular Signatures Database with the fgsea R package (1.16.0).

Ex vivo first-trimester villous explant culture and EVT outgrowth measurement

Extravillous explants (2–3 mm) were obtained from the tips of first-trimester human villi and maintained in 24-well culture dishes precoated with growth factor-reduced Matrigel substrate (Corning, 354230). These explants were cultured in DMEM (Gibco, 11995040) containing 10% (vol/vol) FBS (Gibco, 10091148) at 3% O_2/5%CO_2/92%N_2 humidified atmosphere at 37 °C. Placental villi anchored on Matrigel (with successful initiation of outgrowth) were used for subsequent experiments. EVT outgrowth and migration from the distal end of the villous tips were recorded daily for up to 2 days. The extent of outgrowth was assessed from images captured using an IX73 inverted microscope (Olympus, Shinjuku City, Tokyo, Japan) and measured at defined positions using ImageJ software. To test the potential influence of BMP6 on BMP2-promoted EVT migration, four wells of explants that were derived from a single villous were transfected with siCtrl or si*BMP6* (GenePharma, Shanghai, China) followed by treatment with human BMP2 protein (25 ng/mL) (R&D, 355-BM-010) or PBS.

Primary human Hofbauer cells (HBCs) isolation and culture

Primary human HBCs were isolated from term placentas as described previously.[30] The placental tissue was gently washed in PBS on a magnetic stirrer for 15 min to remove blood and maternal uterine cells. After removing any visible blood clots with forceps, the placental tissue was digested with pre-warmed 0.2% trypsin (Gibco, 25200056)/0.02% EDTA at 37 °C with gentle stirring for 10–15 min. Then, DMEM containing 20% FBS was added to arrest trypsin digestion. The disaggregated cell suspension was filtered through a muslin gauze and centrifuged at 120 g for 5 min at room temperature followed by resuspension of the cell pellet in PBS. Undigested tissue was retrieved from the gauze and further digested with 1 mg/mL collagenase V (Sigma–Aldrich, C9263) supplemented with 40 μg/mL DNase I (Roche, 10104159001) for 40–60 min at 37 °C with gentle shaking. The resultant cell suspension was filtered, centrifuged and resuspended in PBS. Cell suspensions from both trypsin and collagenase digests were combined. Cells were layered onto a Ficoll gradient (GE Healthcare Life Science, 17144002) and centrifuged for 20 min at 600 g, room temperature, acceleration 0, break 1. The leukocyte layer was collected and incubated with antibody cocktail (CD3, FITC; CD14, PE-Dazzle 594; CD19, FITC; CD20, FITC; CD45, PerCP-Cy5.5; CD66b, FITC; CD335, FITC; FOLR2, APC; HLA-A2, APC-Cy7) on ice for 20 min. Cells were washed with FACS buffer (PBS containing 2% FBS and 2 mM EDTA) and resuspended for FACS sorting. Representative images of the gating strategy used for sorting HBCs were presented in Fig. S2. The sorted cells were counted and cultured in macrophage medium (ScienCell, 1921) supplemented with 5% FBS (ScienCell, 0025) and macrophage growth supplements (ScienCell, 1972) at a density of 1×10^6 cells/mL.

Culture of HTR8/SVneo immortalized human EVT cells

The HTR8/SVneo immortalized human EVT cell line (ATCC, CRL-3271, RRID:CVCL_7162) was cultured in

DMEM containing 10% FBS, 100 U/mL penicillin and 100 μg/mL streptomycin (HyClone, SV30010) and incubated at an atmosphere of 5% CO_2 (95% humidity) at 37 °C. To avoid possible interference of growth factors from FBS, cells were maintained in DMEM supplemented with 0.1% (vol/vol) FBS, 100 units/mL penicillin, and 100 μg/mL streptomycin for 24 h before recombinant protein treatment. Cell line was validated and relevant documentation is shown in the Supplemental Data (Reagent and Cell Line Identification File).

Small interfering RNA (siRNA) transfection

Cells at approximately 50% confluency were transfected for 48 h with 20 nM ON-TARGET*plus* SMARTpool siRNA targeting human-specific genes or non-targeting control siRNA (Dharmacon) using Lipofectamine RNAiMAX (Thermo Fisher, 13778-150) and Opti-MEM I (Gibco, 31985070) according to the manufacturer's instructions. Knockdown efficiency was assessed by qPCR or immunoblotting.

Endothelial-like tube formation assay

Growth factor-reduced Matrigel (Corning, 354230) was thawed on ice overnight and diluted 1:1 (vol/vol) with DMEM containing 0.1% FBS. Then, 50 μL diluted Matrigel was added to each well of a 96-well plate and incubated at 37 °C for 2 h to solidify. HTR8/SVneo cells were pre-treated with vehicle or BMP6 (50 ng/mL) for 20 min, and then wells were seeded with 3×10^4 cells suspended in 50 μL vehicle/BMP6-containing DMEM supplemented with 0.1% FBS and incubated at 37 °C for 12 h. Digital images were taken with an Olympus IX73 inverted microscope, and total tube length was measured with ImageJ software.

Matrigel-coated transwell invasion assays

Cell invasiveness was measured using 24-well Transwell inserts (pore size 8 μm; Corning, 3422) coated with 40 μL growth factor-reduced Matrigel at a concentration of 1 mg/mL. Inserts were seeded with 8×10^4 cells in 250 μL DMEM supplemented with 0.1% (vol/vol) FBS, and 750 μL medium with 10% (vol/vol) FBS was added to the lower chamber. Cells were incubated at 37 °C for 36 h, after which non-invading cells were wiped from the upper side of the membrane, and cells on the lower side were fixed with cold methanol (–20 °C) and air-dried. Cell nuclei were stained with Hoechst 33258 (Abcam, ab228550) and imaged with an Olympus IX73 inverted microscope followed by analysis with ImageJ. Triplicate inserts were used for each individual experiment, and five random microscopic fields were counted per insert.

Immunofluorescence

For paraffin section immunofluorescence, the sections were deparaffinized and rehydrated prior to antigen retrieval and primary antibody incubation. For cells grown in cultures, cell masses were fixed with 4% paraformaldehyde in PBS, permeabilized with 0.2% Triton X-100, and blocked with 10% goat serum before antibody staining. Specific primary antibodies were added at a 1:200 dilution overnight at 4 °C. Fluorescent staining was developed using Alexa Fluor 488 (Thermofisher, A11001) or Alexa Fluor 594 (Thermofisher, A11012). The sections were then cover-slipped with anti-fade mounting medium with 4′,6-diamidino-2-phenylindole (DAPI) (Thermofisher, P36935). Fluorescent images were collected by a Dragonfly spinning disc confocal microscope system (Oxford Instruments, Abingdon, UK). ImageJ was used for image analysis.

Immunoblotting

Cells and placentas were lysed in ice-cold cell lysis buffer (Cell Signaling Technology, 9803) and RIPA lysis buffer (Beyotime, P0013B), respectively, with added protease/phosphatase inhibitor cocktail (Cellular Signaling Technology, 5872). Protein concentrations were determined using a BCA protein assay kit (Thermo Fisher, 23235). The immunoblotting was performed as previously described.[27] The antibodies used are listed in Supplementary Table S1. All primary antibodies were diluted by 1:1000 except BMPR2 was diluted by 1:2000. Bound antibodies were visualized using HRP-conjugated secondary antibody, ECL chemiluminescent substrates (Millipore, WBKLS0500), and a Chem-iDoc MP Imaging System (Bio-Rad, Hercules, CA, USA). Membranes were stripped with stripping buffer (Invent Biotechnologies, WA-00350) and reprobed with anti-α-Tubulin antibody (1:5000) as a loading control. Densitometric quantification was performed using ImageJ.

Quantitative PCR (qPCR)

Total RNA was extracted from HTR8/SVneo cells or homogenized placental tissues with TRIzol Reagent according to the manufacturer's instructions. Reverse transcription was performed using 2 μg total RNA and Prime Script RT reagent Kit (Takara Bio, RR047A). qPCR was performed on a Roche LightCycle 480 instrument (Roche, Basel, Switzerland). The primers used are listed in Supplementary Table S2. The specificity of each assay was confirmed by dissociation curve analysis and agarose gel electrophoresis of PCR products. Assay performance was validated by assessing amplification efficiencies by means of calibration curves and ensuring that the plot of log input amount versus ΔCq has a slope with an absolute value of <0.1. Combined results are from at least three independent experiments, wherein each sample was assayed in triplicate and a mean value was used for relative quantification of mRNA levels by the comparative Cq method (with *GAPDH* or *Gapdh* as the reference gene) and using the formula $2^{-\Delta\Delta Cq}$.

EdU proliferation assay

2.5×10^3 HTR8/SVneo cells were seeded in each well of a 96-well plate and cell viability was assessed using a Cell-Light EdU Apollo 567 In Vitro Kit (RiboBio, C10310-1) according to the manufacturer's instructions, with three independent replicates for each treatment group. Images were captured using an IX73 inverted microscope and three fields per well were counted using ImageJ.

TUNEL apoptosis assay

HTR8/SVneo cells were treated with BMP2 (25 ng/mL) or BMP6 (50 ng/mL) and incubated for 36 h followed by 4% paraformaldehyde fixation for 25 min. A permeabilization step was then completed using 1% Triton X-100 in PBS for 5 min. TUNEL staining was performed using a TUNEL kit (Keygen, KGA7063) according to the manufacturer's instructions. Finally, cell nuclei were stained with Hoechst 33258 and imaged with an IX73 inverted microscope followed by analysis with ImageJ. Triplicate wells were used for each individual experiment, and five random microscopic fields were counted per well to determine the TUNEL-positive cell percentage, which was calculated by dividing total number of TUNEL-positive nuclei by total number of nuclei.

Statistics

The sample size in animal study was determined by power analyses based on our pilot experiment. The calculation used the following formula: $n = (2 \times (Z_{\alpha/2} + Z_{\beta})^2 \times \delta^2)/d^2$ [31] with the parameters $\alpha = 0.05$, $\beta = 0.2$, $Z_{\alpha/2} = 1.96$, $Z_{\beta} = 0.84$, $\delta = 4.04$ mmHg (standard deviation of systolic blood pressure), and $d = 10$ mmHg (mean difference of SBP between groups). To minimise potential confounders, the order of treatments and measurements, as well as cage location were also randomized. Experimenters were unblinded to group assignment and outcome assessment. No exclusion criteria were applied. For details on statistical analysis, the number of samples or repeats used for each experiment, and summaries of statistical outputs, see the corresponding Figure legends and Results section. Statistical analysis of bulk RNA-seq and ChIP-seq results is presented in the Methods section for each sequencing technique. In detail, Wald test with Benjamini-Hochberg adjustment implemented in DESeq2 R package with default settings[32] was used to assess the significance of coefficients in regression models for bulk RNAseq data analysis, with the rationale to control the false discovery rate (FDR) when conducting multiple hypothesis tests. Wilcoxon rank-sum test with Bonferroni correction implemented in Seurat R package with default settings[33] was used to compare the distributions of two independent groups for single-cell RNA-seq data analysis, with the rationale to control the family-wise error rate (FWER) when comparing multiple pairs of groups. Multiple group comparison was performed by one-way analysis of variance (ANOVA) or two-way ANOVA followed by the Bonferroni correction for pairwise comparisons. The pROC R package (1.17.0.1) was used to generate receiver operating characteristic (ROC) curves. Shapiro–Wilk test and Q–Q plot were used to assess the normality of data. Levene's test was used to assess the homogeneity of variances among groups. For non-normally distributed data, Mann–Whitney U test was performed. Correlation analysis was performed using Spearman rank correlation analysis. For normally distributed data, group comparisons were performed by ANOVA or t-test. The two factors used in the two-way ANOVA were either siRNA treatment (siCtrl vs. siBMP6) or the adenoviral treatment (Ad Fc vs. Ad Flt-1) and the BMP2 condition (with or without BMP2 supplementation). All bar graphs represent the mean with 95% confidence interval (CI) from at least 3 independent experiments unless stated otherwise.

Ethics

All animal husbandry and procedures were approved by the Ethics Committee and performed in accordance with the Animal Care and Use Committee Guidelines of Shandong University (Approve No. SULCLL2021-2-13). The human studies were approved by the School of Medicine Ethics Board of Shandong University, Jinan, China (Approve No. SDULCLL2021-1-15) and were performed in compliance with the Declaration of Helsinki Principles. All samples were acquired after written informed consent was obtained.

Role of the funding source

The funder of this work had no role in the study design, data collection, data analysis, data interpretation, writing of the report, or decision to submit the article for publication.

Results

BMP2 and EZH2 target genes are aberrantly regulated in preeclamptic placentas

To gain a global view of transcriptome changes in preeclamptic placentas, we performed bulk RNA sequencing (RNA-seq) of placentas from 7 (of 42) healthy pregnant women and from 7 (of 27) women with PE (Fig. 1a–c and Fig. S1a-b). The baseline characteristics of the participants are summarized in Table 1. Among a total of 2278 differentially expressed genes (DEGs) ($p < 0.05$), genes including *FLT1*, *LEP*, *HTRA4*, and *SYNPR*, have been previously reported as PE-related (Fig. 1b).[25,34–36] We further ranked the 2278 DEGs based on a t-statistic and performed Gene Set Enrichment Analysis (GSEA) using the Molecular Signatures Database (MSigDB).[37,38] The top differentially enriched pathways, including TNFα signalling, hypoxia,

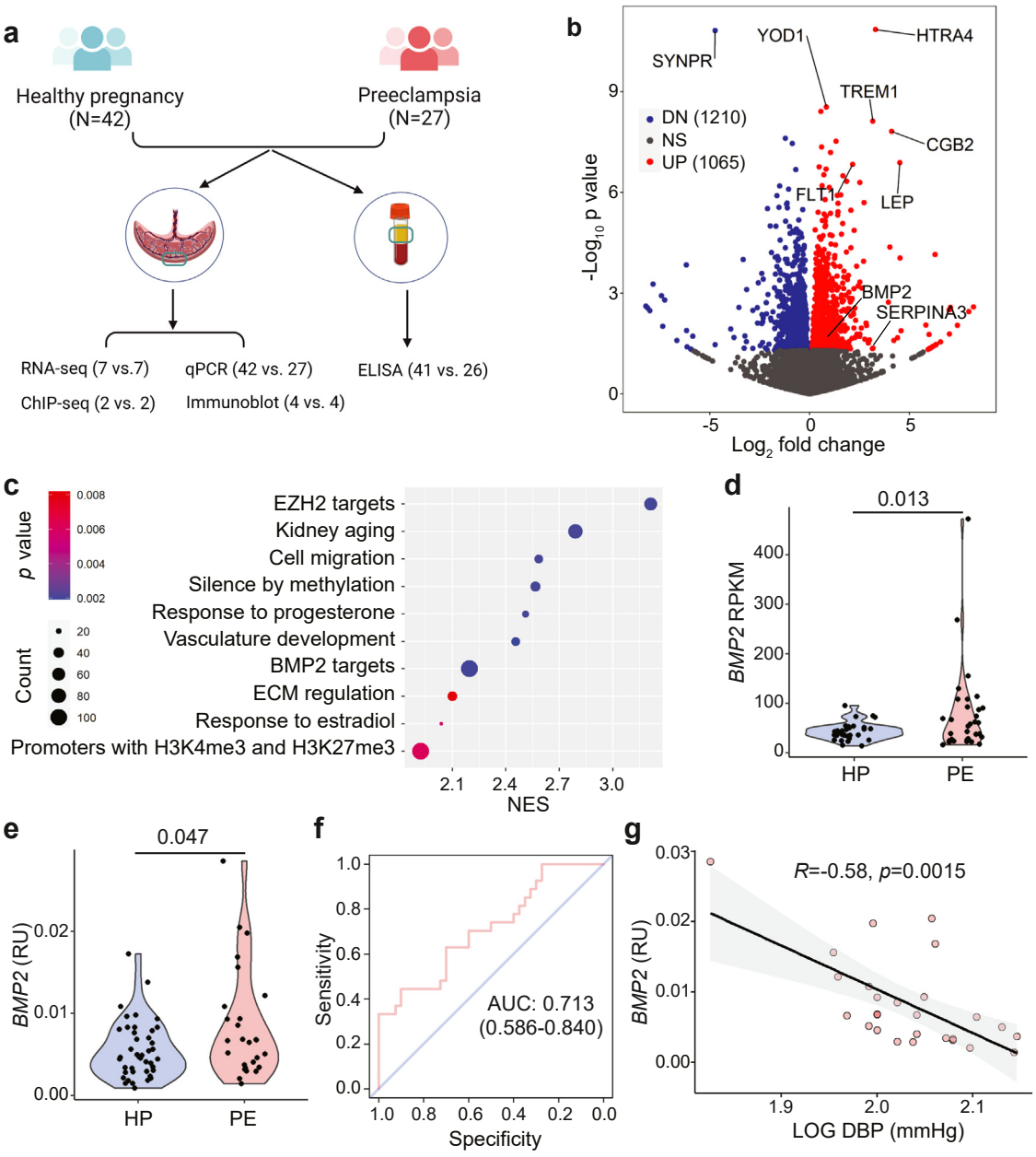

Fig. 1: **BMP2 signalling is increased in preeclamptic placentas and negatively associated with the severity of clinical manifestations.** **a**, Schema showing the design of clinical study in the present study. **b**, Volcano plot of RNA-seq data showing the most differentially expressed genes (DEGs) in preeclamptic placentas vs healthy placentas (n = 7 in each group). Significantly regulated genes above and below two-fold are shown in red and blue, respectively. DEGs previously reported as related to PE are labeled. **c**, Dot plot of significantly enriched Gene Ontology (GO) terms in preeclamptic placentas compared to healthy placentas. Dot size represents the number of DEGs from a particular GO term (count), and the color depicts the p value. **d**, The *BMP2* expression in preeclamptic and healthy placentas from a published RNA-seq database with a larger cohort (n = 30 in each group). **e**, qPCR analysis of *BMP2* expression in preeclamptic and healthy placentas (N = 42 vs. 27) using *GAPDH* as the reference gene. **f**, Receiver operating characteristic (ROC) curve for placental *BMP2* expression as a diagnostic marker for PE. AUC with 95% CI is labeled. **g**, Spearman correlation analysis between the mRNA levels of *BMP2* in preeclamptic placentas and the clinical diastolic blood pressure (DBP) of the corresponding patients. The gray area represents 95% CI. Each dot donates one sample. Adjusted p value by Wald test with Benjamini-Hochberg adjustment is labeled in (**d**). DESeq2 by default employs the Wald test on raw count data to identify differential gene expression, and adjusts p values via the Benjamini-Hochberg method to control false discovery rate. p value by Mann–Whitney U test is labeled in (**e**).

and epithelial–mesenchymal transition, have been previously reported as PE-related (Fig. S1a).[20,39,40] Notably, the Gene Ontology (GO) terms BMP2 targets and EZH2 targets were also significantly enriched (Fig. 1c).

We further explored the GSEA Molecular Signatures Database and identified additional genes putatively related to BMP2 signalling and EZH2 modification. Interestingly, we found that *BMP2* and 50 genes of the 206 previously reported BMP2 target genes were regulated by EZH2 modification (Fig. S1b).[41–46] Given that EZH2 is the catalytic subunit of PRC2 which induces H3K27me3, these findings suggest that H3K27me3-related epigenetic mechanisms may be involved in the regulation of BMP2 signalling in preeclamptic placentas.

BMP2 is upregulated in preeclamptic placentas and its level is negatively correlated with the severity of clinical manifestations

Consistent with enriched BMP2 targets, we found that *BMP2* was significantly up-regulated in the PE placentas (Fig. 1b). To corroborate our findings, we turned to a published PE placenta bulk RNA-seq database with a larger cohort (n = 30 vs. 30).[47] We re-analyzed their data and found *BMP2* was also significantly up-regulated (Fig. 1d). qPCR was also used to assess additional preeclamptic and healthy placentas in our cohort (n = 27 vs. 42), and the significantly increased *BMP2* level in the preeclamptic placentas was consistently observed (Fig. 1e). ROC curve analysis was then performed to calculate *BMP2*'s diagnostic value for PE: the area under the curve (AUC) for this was 0.713, indicating an acceptable diagnostic ability (Fig. 1f).[48] We also performed Spearman correlation analysis examining *BMP2* mRNA levels in preeclamptic placentas and patients' diastolic blood pressure (DBP). Although an increased *BMP2* level was observed in preeclamptic placentas, the expression levels of *BMP2* were negatively correlated with DBP (Fig. 1g).

The average gestation age of preeclamptic placentas was 33.1 weeks, while the average gestational age of healthy placentas was 37.6 weeks (Table 1). To assess whether the increased *BMP2* levels we observed in preeclamptic placentas were potentially biased due to gestational age differences, immunoblotting was performed to examine BMP2 protein levels in preterm and term placentas of healthy pregnancies. We detected comparable levels of BMP2 in preterm and term placentas (Fig. S1c), arguing against bias in our data resulting from different gestational ages between healthy and preeclamptic placentas. Importantly, given multiple previous studies showing that BMP2 promotes trophoblast invasion by increasing trophoblast invasiveness and vascular mimicry ability,[12,49,50] the negative correlation we detected could be interpreted to indicate that increased BMP2 may represent a self-compensatory mechanism for shallow trophoblast invasion in PE.

Genome-wide H3K27me3 is decreased in preeclamptic placentas

To profile the aberrant genome-wide H3K27me3 modifications in preeclamptic placentas, we performed ChIP-seq. A GSEA of genes with differential H3K27me3 peaks indicated that promoters with H3K27me3 were the most significantly enriched gene set (lowest p value) in the ChIP-seq dataset (Fig. 2a).[45] Response to BMP was also significantly enriched, indicating that BMP signalling was aberrantly regulated by H3K27me3 modification in preeclamptic placentas (Fig. 2a). There was also enrichment among the differentially H3K27me3-modified loci for genes encoding proteins with functional annotations related to SMAD protein signal transduction and TGF-β receptor signalling (Fig. 2a). Next, we quantified the H3K27me3 signal across the ± 3-kb regions from the transcription start sites (TSSs) of genes with at least one differentially enriched chromatin peak. The H3K27me3 density at these regions was significantly lower in preeclamptic placentas than in healthy placentas (Fig. 2b and Fig. S1d), reflecting a clear trend of H3K27me3 alteration in preeclamptic placentas.

BMP2 locus is modified by H3K27me3 in Hofbauer cell which is the origin of BMP2 in placenta

Integrative Genomics Viewer (IGV) tracks for ChIP-seq showed an enriched peak for H3K27me3 at the TSS region of the *BMP2* locus and a reduced extent of H3K27me3 modification at the *BMP2* locus in the preeclamptic placentas compared to the healthy placentas (Fig. 2c). These results suggest that decreased H3K27 trimethylation at the *BMP2* promoter region may be responsible for the increased *BMP2* expression reported for preeclamptic placentas.[22] To validate the increased BMP2 and decreased H3K27me3 levels in preeclamptic placentas from our RNA-seq and ChIP-seq datasets, we performed immunoblotting to quantify the BMP2 and overall H3K27me3 levels in additional healthy and preeclamptic placentas. Briefly, the BMP2 protein level was significantly higher in preeclamptic placentas than in healthy placentas, while the H3K27me3 level was significantly lower in preeclamptic placentas than in healthy placentas (Fig. 2d and e). Note that we also detected comparable levels of H3K27me3 in preterm and term placentas (Fig. S1c), precluding the possibility that the trends in our data reflect different gestational ages between the healthy and preeclamptic placentas.

To pinpoint the cellular source of BMP2 in placenta, we integrated two already-published, single cell RNA-seq datasets of placentas from 5 healthy donors and 5 PE donors.[28,29] The characteristics of donors are summarized in Supplementary Table S3. Using markers established in these previous studies, we captured majority of cell types in placenta (Fig. 2f).[51] We found that Hofbauer cells, the placental villous macrophages of fetal origin that are present throughout pregnancy,[52]

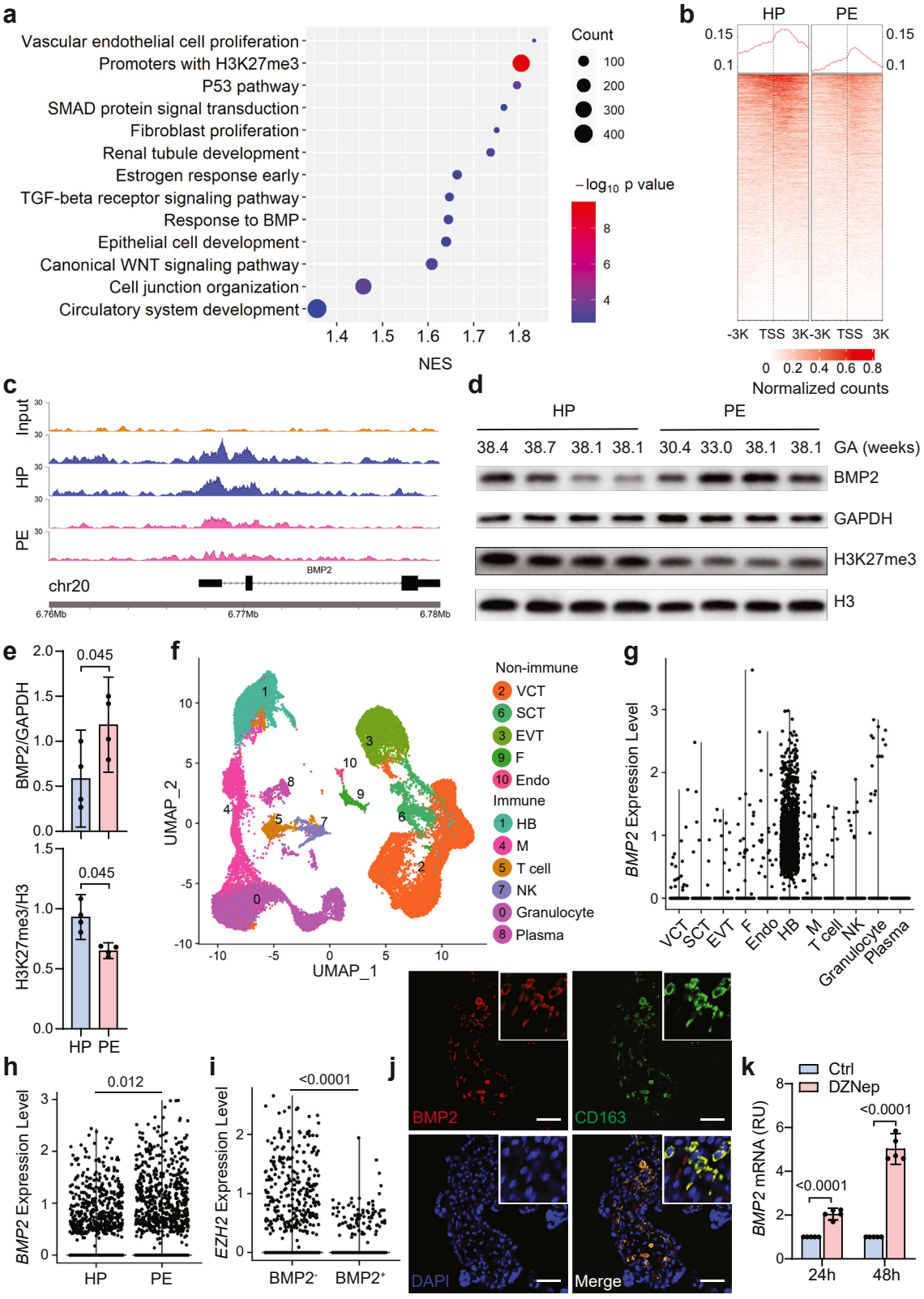
a
Vascular endothelial cell proliferation
Promoters with H3K27me3
P53 pathway
SMAD protein signal transduction
Fibroblast proliferation
Renal tubule development
Estrogen response early
TGF-beta receptor signaling pathway
Response to BMP
Epithelial cell development
Canonical WNT signaling pathway
Cell junction organization
Circulatory system development
1.4 1.5 1.6 1.7 1.8
NES
Count
100
200
300
400
−log10 p value
8
6
4
b
HP
PE
0.15
0.1
-3K TSS 3K-3K TSS 3K
0 0.2 0.4 0.6 0.8
Normalized counts
c
Input
HP
PE
BMP2
chr20
6.76Mb
6.77Mb
6.78Mb
d
HP
PE
38.4 38.7 38.1 38.1 30.4 33.0 38.1 38.1 GA (weeks)
BMP2
GAPDH
H3K27me3
H3
e
BMP2/GAPDH
0.045
H3K27me3/H3
0.045
HP PE
f
UMAP_1
UMAP_2
Non-immune
2 VCT
6 SCT
3 EVT
9 F
10 Endo
Immune
1 HB
4 M
5 T cell
7 NK
0 Granulocyte
8 Plasma
g
BMP2 Expression Level
VCT SCT EVT F Endo HB M T cell NK Granulocyte Plasma
h
BMP2 Expression Level
0.012
HP PE
i
EZH2 Expression Level
<0.0001
BMP2- BMP2+
j
BMP2
CD163
DAPI
Merge
k
Ctrl
DZNep
BMP2 mRNA (RU)
<0.0001
<0.0001
24h 48h

were the main source of BMP2 in placenta (Fig. 2g). Double staining of placenta sections with BMP2 and CD163, a macrophage marker,[51,52] confirmed Hofbauer cells as the origin of BMP2 (Fig. 2j). In addition, we found that the level of *BMP2* in Hofbauer cells from PE patients was significantly higher than that in Hofbauer cells from healthy controls (Fig. 2h), reinforcing our findings from the bulk RNA-seq analyses of placenta. Of note, we found that the *EZH2* level in *BMP2*$^{+}$ Hofbauer cells was significantly decreased compared to that in *BMP2*$^{-}$ Hofbauer cells (Fig. 2i). In combination with our ChIP-seq and immunoblotting data in placenta (Fig. 2c–e), we speculate that decreased H3K27me3 at the *BMP2* locus may account for the observed increase in the *BMP2* levels in Hofbauer cells from PE patients.

We experimentally pursued this by working with primary cultures of human Hofbauer cells that were isolated from term placentas[30] (Fig. S2). Primary Hofbauer cells were treated for 24 h or 48 h with or without 2 μM 3-deazaneplanocin A (DZNep), which inhibits EZH2's function in catalyzing the addition of methyl groups at H3 lysine 27.[53] qPCR showed that DZNep treatment significantly increased *BMP2* mRNA levels in a time-dependent manner (Fig. 2k). Collectively, these results support that a decreased extent of H3K27me3 at the *BMP2* locus can increase the BMP2 level in Hofbauer cells.

BMP2 upregulates trophoblast invasion and increases the expression of BMP6, which is associated with preeclampsia

As a secretory molecule, BMP2 has been identified as a pro-invasive factor during human trophoblast differentiation; it promotes human trophoblast invasion and vascular mimicry.[12,49] To explore BMP2-induced phenotypes of human trophoblast cells and examine potential molecular targets of BMP2, we used RNA-seq to profile the transcriptomes of immortalized human trophoblast HTR8/SVneo cells that were treated with or without BMP2 for 6 or 24 h (Fig. 3a–g). The clear separation in a principal component analysis (PCA) scores plot indicated that BMP2 treatment could obviously alter trophoblast transcriptome (Fig. 3a–b). Among many trophoblast- and PE-associated DEGs, several genes including *ID1-4*, *PGF*, *MMP2*, *MMP11*, and *MMP14* merit specific emphasis. Inhibitor of differentiation (ID) proteins have been reported as BMP2 targets that function in trophoblasts to promote invasive differentiation[49,54]; here, we found that *ID1*, *ID2*, *ID3*, and *ID4* were among the top-ranking DEGs upon BMP2 treatment (Fig. 3c). The *PGF* gene encodes placental growth factor (PlGF), an essential molecule in the prediction, diagnosis, and treatment of PE.[55] *PGF* was also among the DEGs and was significantly upregulated in trophoblasts after BMP2 treatment (Fig. 3c). Moreover, many genes encoding matrix metalloproteinases including *MMP2*, *MMP11*, and *MMP14*, which are essential for degrading decidual extracellular matrix proteins and thereby facilitating cell invasiveness,[56] were also significantly upregulated by BMP2 treatment (Fig. 3d and e).

GSEA showed that response to BMP, response to TGF-β, and targets of SMAD2 and SMAD3 were enriched in the transcriptome of trophoblasts treated with BMP2 (Fig. 3f).[8] Components of the Notch, Wnt, RhoA, Rb1, and SMARCE1 signalling pathways, which are each known to function in hierarchical vascular network establishment,[56–60] were significantly enriched (Fig. 3f). GSEA in the GO term database showed significant enrichment for terms including epithelial proliferation, differentiation, development and morphogenesis, epithelial–mesenchymal transition (EMT), endothelial development and cell migration, and artery development and morphogenesis, which are all essential for trophoblast invasion and vascular mimicry (Fig. 3g).[20] Taken together, this transcriptome analysis indicates that BMP2 regulates multiple trophoblast invasion- and vascular mimicry-related events.

Interestingly, *BMP6* was among the top-ranking upregulated DEGs after BMP2 treatment (Fig. 3c). We also treated HTR8/SVneo cells with BMP2 for different lengths of time and with different doses. Briefly, qPCR showed that BMP2 increased the *BMP6* mRNA level in a time- and dose-dependent manner (Fig. 3h and i),

Fig. 2: **BMP2 is derived from Hofbauer cells and aberrantly regulated by H3K27me3 modification in preeclamptic placentas**. **a-c**, Genome-wide H3K27me3 mapping by ChIP-seq in 2 preeclamptic placentas and 2 healthy placentas. **a**, Gene set enrichment analysis (GSEA) using the 2009 genes with at least one enriched peak for H3K27me3 histone modification in the ChIP-seq dataset. Dot size represents the number of genes with at least one enriched peak from a particular gene set (count), and the color depicts the p value. **b**, Heatmaps for ± 3 kb region around transcription start site (TSS) of the 2009 genes with enriched H3K27me3 ChIP signals. **c**, Genomic snapshots of H3K27me3 ChIP-seq data for the *BMP2* locus in preeclamptic and healthy placentas. **d** and **e**, Immunoblotting against BMP2 and H3K27me3 in preeclamptic and healthy placentas normalized to the GAPDH and H3 signals, respectively. **f-i**, Two published single cell transcriptomes of placentas from 5 preeclamptic donors and 5 healthy donors were integrated and re-analyzed. **f**, t-SNE plot displays all captured cell types. **g**, Violin plot displays the *BMP2* expression level in all cell types. **h**, Violin plot displays the *BMP2* expression level in Hofbauer cells from preeclamptic and healthy placentas. **i**, Violin plot displays the *EZH2* expression level in *BMP2*$^{+}$ and *BMP2*$^{-}$ Hofbauer cells. **j**, Immunofluorescence staining of BMP2 and CD163 in healthy placentas. Scale bar, 40 μm. **k**, Human primary Hofbauer cells were treated with an EZH2 inhibitor (DZNep; 2 μM) for the indicated durations, and *BMP2* mRNA levels were examined with qPCR using *GAPDH* as the reference gene. Each dot donates one sample and quantitative results are expressed as mean with 95% CI. Adjusted p values by non-parametric Wilcoxon rank sum test with Bonferroni correction are labeled in (**h, i**). p values by two-tailed Student's t test are labeled in others.

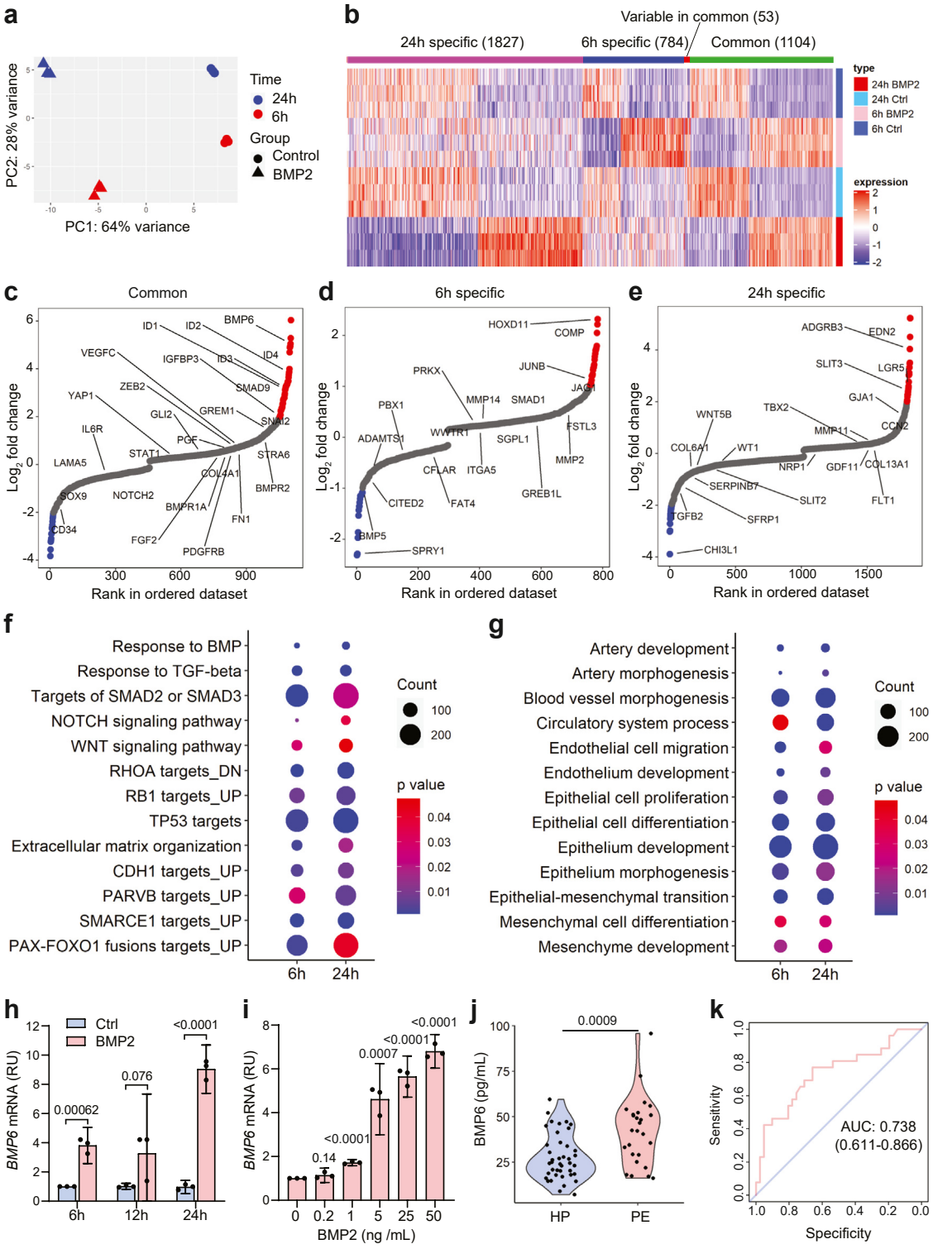

Fig. 3: **BMP2 transcriptionally activates an anti-preeclampsia transcription program and BMP6 is increased in the serum of preeclamptic patients**. a-g, HTR8/SVneo cells were treated with or without 25 ng/mL BMP2 for 6 h or 24 h prior to RNA-seq. **a**, PCA showing the separation between samples from the four experimental groups. **b**, Heatmap depicting DEG (adjusted p value < 0.05) signatures: "6 h specific" refers to genes only differentially expressed after 6 h BMP2 treatment; "24 h specific" for genes only differentially expressed after 24 h BMP2 treatment;

confirming that *BMP6* transcription is upregulated by BMP2 treatment in human trophoblasts. In addition, we detected significantly increased BMP6 levels in the third-trimester sera of preeclamptic patients as compared to healthy pregnancies (n = 41 vs. 26) (Fig. 3j); the BMP2 levels were barely detectable in these sera samples. ROC curve analysis indicated that BMP6 (AUC = 0.738) serve as a candidate circulating biomarker for PE occurrence (Fig. 3k).

BMP6 mediates basal and BMP2-promoted human trophoblast invasion

We next aimed to identify the roles of BMP6 in basal and BMP2-increased human trophoblast invasion and vascular mimicry. We first treated HTR8/SVneo cells with human recombinant BMP6 protein for both Transwell invasion assays and endothelial-like tube formation assays. BMP6 significantly promoted the invasiveness of HTR8/SVneo cells (Fig. 4a) and promoted the extent of vascular mimicry as assessed by total branching points and tube length (Fig. 4b), indicating the pro-invasive role of BMP6 in human trophoblast.

We then treated HTR8/SVneo cells with BMP6 for 6 or 24 h and conducted RNA-seq analysis. A PCA indicated that the BMP6-treated cells had obviously distinct transcriptomes compared to the PBS controls (Fig. 4c). The levels of *ID1*, *ID2*, *ID3*, *ID4*, *PGF*, and many other PE-related genes were significantly altered after BMP6 treatment (Fig. 4d and Fig. S3a–c). Similar to BMP2 treatment, BMP6 treatment of trophoblasts significantly changed genes enriched in epithelial proliferation, differentiation and development, epithelial–mesenchymal transition, mesenchymal cell differentiation, endothelial development and cell migration, and artery development and morphogenesis (Fig. 4e). To examine whether BMP6 activates canonical and/or non-canonical TGF-β signalling pathways, HTR8/SVneo cells were treated with BMP6 for different durations and dosages. Immunoblotting showed that BMP6 treatment activated both the p-SMAD2/3 and p-SMAD1/5/9 pathways, doing so in a dose-dependent manner within 60 min of treatment (Fig. S3d and e); no influence of BMP6 treatment was detected for the p-ERK, p-AKT, or p-FAK pathways (Fig. S3f).

To examine whether BMP6 is required for the observed effects of BMP2 on human trophoblast invasion and vascular mimicry, we performed Transwell invasion assays, endothelial-like tube formation assays, and first-trimester villous explant outgrowth assays with a combination of BMP2 treatment and siRNA-mediated *BMP6* knockdown. Consistent with previous findings,[12,49] we found that BMP2 treatment significantly promoted both human trophoblast invasion and vascular mimicry. siRNA-mediated *BMP6* knockdown abolished both the BMP2-induced pro-invasive effect and vascular mimicry as examined with Transwell invasion assays and endothelial-like tube formation assays (Fig. 4f–h). Moreover, *ex vivo* experiments using first-trimester villous explants again supported a mediation role of BMP6 in BMP2-promoted trophoblast migration, as knockdown of *BMP6* in villous explants abolished BMP2's pro-migration effect (Fig. 4i). Of note, no difference in the proliferation or apoptosis rates of HTR8/SVneo cells was detected upon BMP2 and BMP6 treatment, or upon siRNA-mediated *BMP6* knockdown (Fig. S3g–j). These results show that BMP6 is required for the observed effects of BMP2 on human trophoblast invasion and vascular mimicry.

BMP2 upregulates BMP6 in a BMPR1A-SMAD2/3-SMAD4-dependent manner

BMPs exert their biological effects primarily via canonical SMAD1/5/9-SMAD4 signalling; however, several reports have demonstrated the mediation roles of non-canonical SMAD2/3-SMAD4 and/or SMAD-independent signalling in BMPs-regulated biological behaviors.[12,61] To assess whether SMAD-dependent signalling is involved in the observed BMP2-upregulated BMP6 expression in human trophoblasts, we measured the phosphorylation of SMAD1/5/9 and SMAD2/3 following treatment of HTR8/SVneo cells with BMP2 for 15, 30, or 60 min. Immunoblotting showed that BMP2 treatment significantly increased

"Common" for genes differentially expressed after both 6 h and 24 h BMP2 treatment, and sharing the same changing trend, and "Variable in common" for genes with opposite changing trends. **c-e**, Waterfall plots showing "Common" DEGs (**c**), "6 h specific" DEGs (**d**), and "24 h specific" DEGs (**e**). The gene lists are ranked by log2 fold change and all dots indicate DEGs. Red dots indicate DEGs with log2 fold change >2 (**c** and **e**) or log2 fold change >1 (**d**). Blue dots indicate DEGs with log2 fold change < −2 (**c** and **e**) or log2 fold change < −1 (**d**). Cutpoints of 1 and 2 for log2 fold change were used in our RNAseq analysis, representing 2-fold and 4-fold changes in gene expression respectively. These thresholds, chosen based on typical standards and our specific experimental design, strike a balance between identifying meaningful biological changes and controlling false positives. **f-g**, Dot plots of significantly enriched pathways (**f**) and GO terms (**g**). Dot size represents the number of DEGs from a particular pathway or GO term (count). **h**, HTR8/SVneo cells were treated with or without 25 ng/mL BMP2 for the indicated durations, followed by qPCR analysis of *BMP6* levels using *GAPDH* as the reference gene. **i**, HTR8/SVneo cells were treated with or without the indicated BMP2 doses for 6 h, followed by qPCR analysis of *BMP6* levels. **j,** BMP6 concentrations in the serum of healthy and preeclamptic pregnant women assayed by ELISA (n = 41 vs. 26). **k**, ROC curve for serum BMP6 level as a diagnostic marker for PE. AUC with 95% CI is labeled. Each dot donates one sample and quantitative results are expressed as the mean with 95% CI. p values by two-tailed Student's t test are labeled in (**h**, **i**) and p value by Mann–Whitney U test is labeled in (**j**).

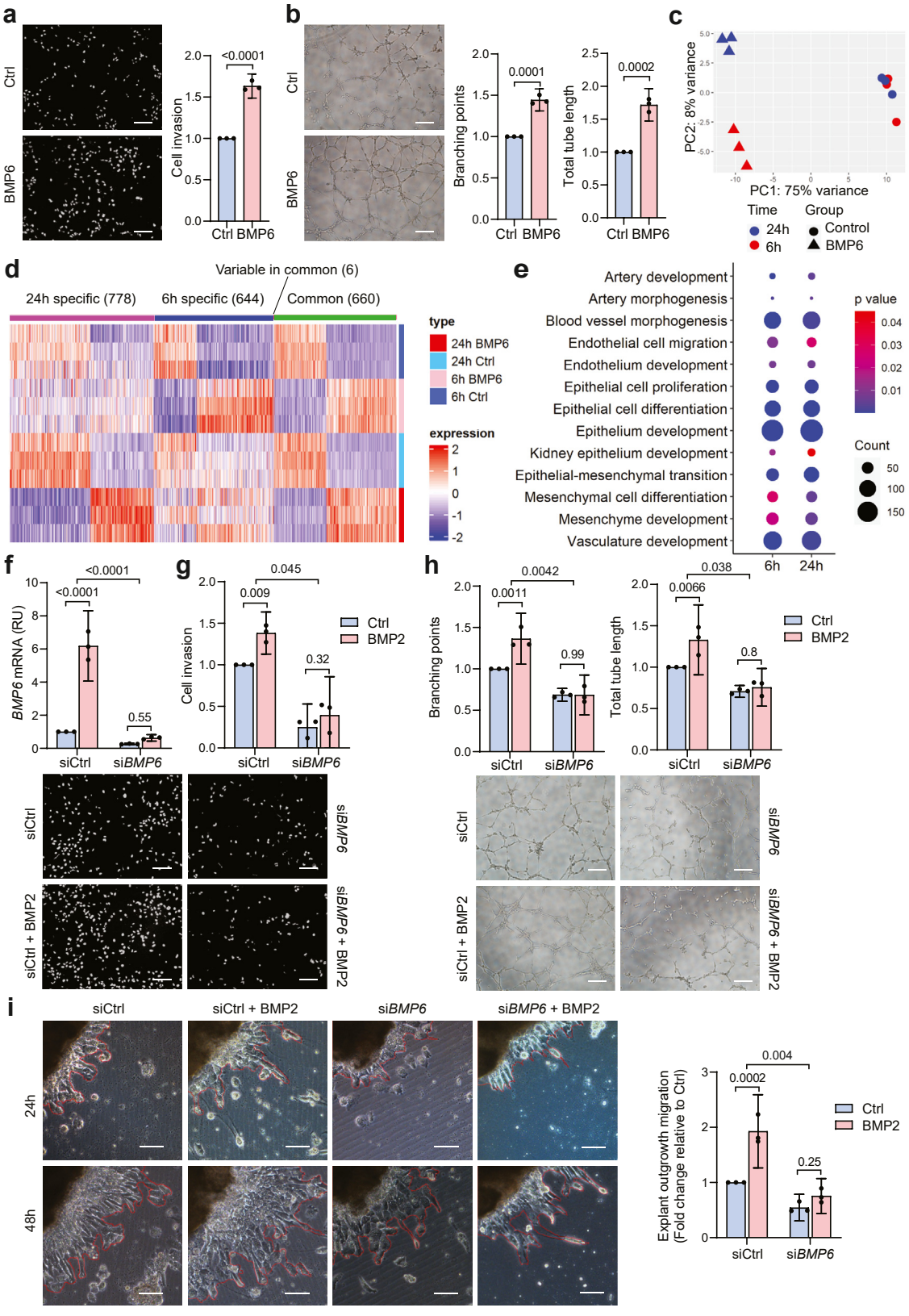
a
Ctrl
BMP6
Cell invasion
<0.0001
Ctrl BMP6
b
Ctrl
BMP6
Branching points
0.0001
Total tube length
0.0002
Ctrl BMP6
c
PC2: 8% variance
PC1: 75% variance
Time
24h
6h
Group
Control
BMP6
d
Variable in common (6)
24h specific (778)
6h specific (644)
Common (660)
type
24h BMP6
24h Ctrl
6h BMP6
6h Ctrl
expression
e
Artery development
Artery morphogenesis
Blood vessel morphogenesis
Endothelial cell migration
Endothelium development
Epithelial cell proliferation
Epithelial cell differentiation
Epithelium development
Kidney epithelium development
Epithelial-mesenchymal transition
Mesenchymal cell differentiation
Mesenchyme development
Vasculature development
6h
24h
p value
Count
f
BMP6 mRNA (RU)
<0.0001
<0.0001
0.55
siCtrl
siBMP6
g
Cell invasion
0.045
0.009
0.32
Ctrl
BMP2
siCtrl
siBMP6
siCtrl + BMP2
siBMP6 + BMP2
h
Branching points
0.0042
0.0011
0.99
Total tube length
0.038
0.0066
0.8
i
siCtrl
siCtrl + BMP2
siBMP6
siBMP6 + BMP2
24h
48h
Explant outgrowth migration (Fold change relative to Ctrl)
0.004
0.0002
0.25

both SMAD1/5/9 phosphorylation and SMAD2/3 phosphorylation (Fig. 5a). HTR8/SVneo cells were further treated with BMP2 following siRNA-mediated knockdown of *SMAD1/5/9* (*SMAD1, SMAD5* and *SMAD9*), *SMAD2/3* (*SMAD2* and *SMAD3*) or *SMAD4*. The efficient knockdown was confirmed by immunoblotting (Fig. S4a and b). Knockdown of *SMAD1/5/9* had no effect, whereas knockdown of *SMAD2/3* or *SMAD4* significantly attenuated BMP2's upregulation of BMP6 (Fig. S4a–c). These findings support a mediation role for SMAD2/3 in BMP2-induced BMP6 upregulation, and the activated SMAD1/5/9 could regulate additional BMP2-downstream targets rather than BMP6.

To investigate which type I receptors of the TGF-β superfamily are involved in BMP2-induced SMADs phosphorylation and BMP6 upregulation, HTR8/SVneo cells were pretreated with or without 1 μM DMH-1 (a known inhibitor of ACVR1 and BMPR1A[62]) or 10 μM SB431542 (a known inhibitor of ACVR1B, TGFβRI and ACVR1C[63]), prior to BMP2 treatment. BMP2-induced phosphorylation of SMAD1/5/9 and SMAD2/3, as well as BMP6 upregulation didn't change after SB431542 treatment (Fig. 5b). The siRNA-mediated *ACVR1B* and *TGFBR1* knockdown didn't change the inductions, either (Fig. 5c and Fig. S4d), precluding the involvement of ACVR1B, TGFβRI or ACVR1C. However, the inductions were completely abolished by treatment with DMH-1 (Fig. 5b and Fig. S4e), further precluding the involvement of ACVRL1 or BMPR1B. Moreover, siRNA-mediated *BMPR1A* knockdown, but not siRNA-mediated *ACVR1* knockdown, abolished BMP2-induced SMADs phosphorylation and BMP6 upregulation (Fig. 5d and Fig. S4f–i); *BMPR1A* was expressed in trophoblast and upregulated upon BMP2 treatment (Fig. 3c and Fig. S4g). Although BMPR2, a type II receptor of the TGF-β superfamily, was also upregulated by BMP2 in a BMPR1A-SMAD2/3-SMAD4-dependent manner (Fig. 3c and Fig. S4j–m), we found that BMPR2 did not mediate BMP2-induced SMADs phosphorylation and BMP6 upregulation (Fig. S4n). Taken together, these results suggest BMPR1A is the functional receptor for BMP2 in trophoblasts.

To confirm the pathological role of the identified BMP2-BMPR1A signalling in PE, we further explored the human placenta single-cell transcriptome to identify the cell-type-specific expression profile of *BMPR1A* at the maternal–fetal interface during pregnancy.[28,29] *BMPR1A* expression was mainly detected in trophoblasts, especially in villous cytotrophoblasts (VCTs) (Fig. 5e). The double staining of placenta section with antibodies against BMPR1A and E-cadherin, a VCT marker,[51] confirmed that BMPR1A was primarily expressed in VCTs, which are lineage progenitors of EVTs and are located in the innermost chorionic villi layer of the placenta (Fig. 5f). As the villous Hofbauer cells are the main origin of BMP2 (Fig. 2g and j), this grants the spatial privilege for the occurrence of BMP2-BMPR1A signalling between Hofbauer cells and VCTs.

We then compared the transcriptome difference between $BMPR1A^+$ VCTs and $BMPR1A^-$ VCTs and consistently found that pro-invasive BMP2 target genes including *ID1*, *ID2*, *ID3*, and *ID4* were among the top-ranking DEGs. Other known PE-related genes including *EGFR, GDF15, COL4A2,* and *XIST* were also significantly up-regulated in $BMPR1A^+$ VCTs (Fig. 5g).[64–66] In addition, EGF signalling, epithelial to mesenchymal transition, TGF-β signalling, vasculature development, and other PE-related events were significantly enriched in GSEA (Fig. 5h), emphasizing the role of BMPR1A, which mediates the effects of BMP2 in the trophoblast invasion process, in the prevention of PE development. The explicit cell-type specific expression profiles of *BMP2* and *BMPR1A* (Figs. 2g and 5e) potentially provide specific targets for PE treatment.

Supplementation with recombinant BMP2 alleviates PE-related phenotypes in an Ad Flt1-induced PE rat model

To explore whether BMP2 upregulation can alleviate PE-related phenotypes *in vivo*, we supplemented

Fig. 4: **BMP6 mediates basal and BMP2-induced human trophoblast invasion and vascular mimicry**. a-b, HTR8/SVneo cells were treated with or without 50 ng/mL BMP6 for 36 h, followed by analysis of cell invasiveness (**a**) and endothelial-like tube formation (**b**). The left panel shows representative images, and the right panel shows summarized quantitative results. Scale bar, 200 μm. **c-e,** HTR8/SVneo cells were treated with or without 50 ng/mL BMP6 for 6 h or 24 h, followed by RNA-seq. **c**, PCA showing the separation between samples. **d**, Heatmap depicting DEG (adjusted p value < 0.05) signatures of each group. The adjusted p value was obtained through the Benjamini-Hochberg procedure, which corrects for multiple comparisons by ranking and recalibrating individual p values, thereby minimizing false positives. **e**, Dot plots of significantly enriched GO terms. Dot size represents the number of DEGs from a particular term (count). **f-h**, Cells were transfected for 48 h with 20 nM non-targeting control siRNA or siRNA targeting *BMP6* prior to treatment with or without 25 ng/mL BMP2 for 6 or 36 h. **f**, *BMP6* mRNA levels were examined by qPCR 6 h after BMP2 treatment. **g**, Cell invasiveness was examined with Transwell assay. The upper panel shows summarized quantitative results; the lower panel shows representative images. Scale bar, 200 μm. **h**, The vascular mimicry phenotype of HTR8/SVneo cells was examined by an endothelial-like tube formation assay. The upper panels show summarized quantitative total branching points and total tube length results, and the lower panels show representative images. Scale bar, 200 μm. **i**, Extravillous explants from first-trimester villi were transfected with 20 nM non-targeting control siRNA or siRNA targeting *BMP6* prior to treatment with or without 25 ng/mL BMP2. The migration distance of villous tips was qualified in the right panel. Scale bar, 100 μm. Each dot donates one sample and data is expressed as the mean with 95% CI. p values by two-tailed Student's t test are labeled in (**a**, **b**) and p values by two-way ANOVA are labeled in (**f–i**).

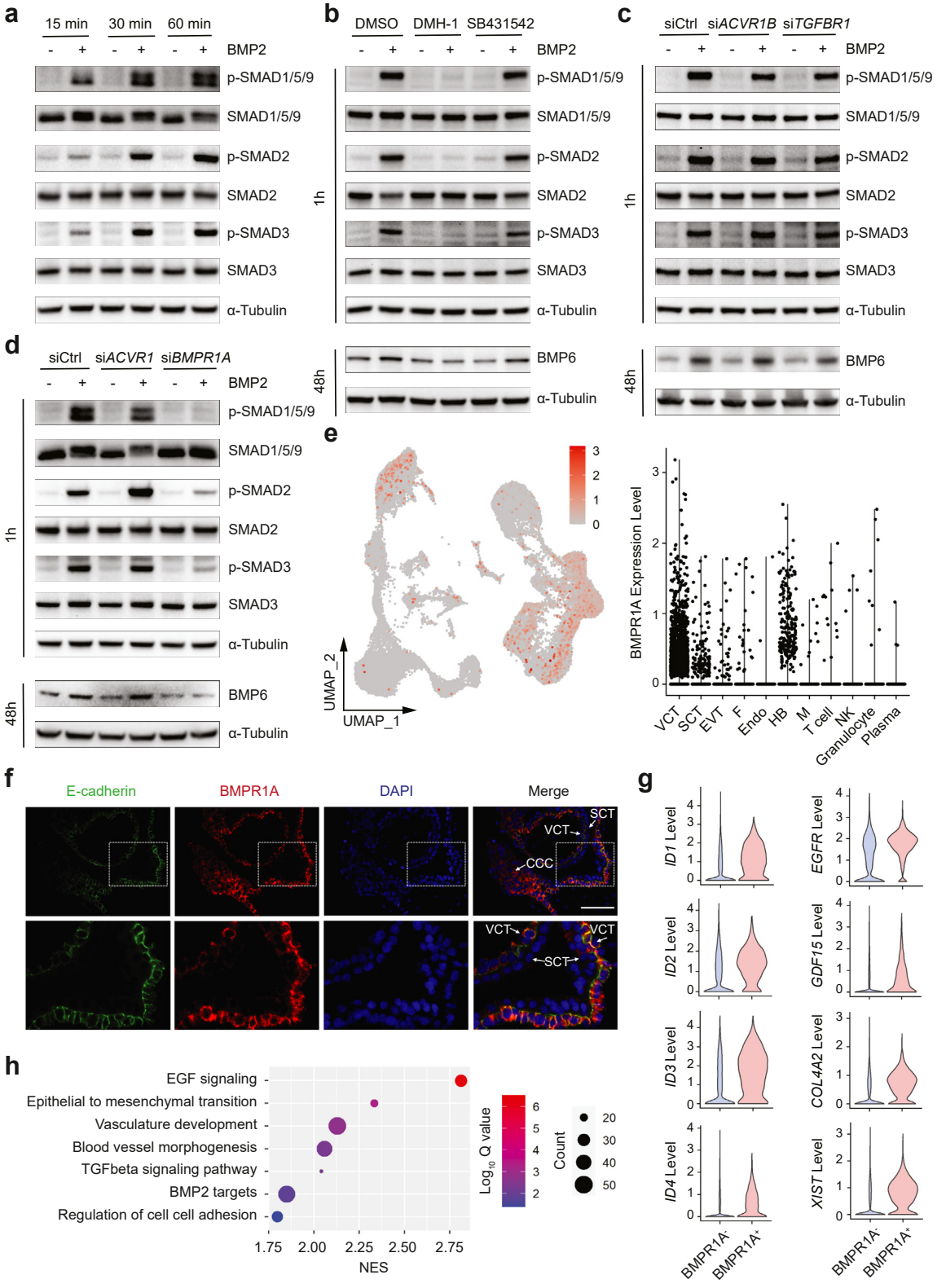

Fig. 5: **BMP2 upregulates BMP6 in trophoblast via BMPR1A-SMAD2/3-SMAD4 signalling**. a, HTR8/SVneo cells were treated with or without 25 ng/mL BMP2 for the indicated durations and the protein levels of targets were assayed by immunoblotting. **b**, HTR8/SVneo cells were

recombinant BMP2 protein to Ad Flt1-induced PE model rats,[67] followed by assessment of PE-related pathological changes and phenotypes, including blood pressure, placental weight, placental labyrinth/junction ratio, and fetal weight, as well as levels of soluble fms-like tyrosine kinase-1 (sFlt-1, also known as soluble VEGFR-1) in plasma and albumin/creatinine in urine (Fig. 6a).[25,68] sFlt-1 expressing adenovirus injection at gestational day 8 (G8) successfully established the PE-like rat model; the animals displayed the anticipated increases in plasma sFlt-1 levels, mean blood pressure, systolic blood pressure, urine albumin/creatinine ratio, and glomeruli damage, as well as decreased placental weight, placental labyrinth/junction ratio, and fetal weight (Fig. 6b–g and Fig. S5a–c). Supplementation with recombinant BMP2 significantly alleviated PE-related phenotypes including increased mean blood pressure and systolic blood pressure as well as decreased placental weight, placental labyrinth/junction ratio, and fetal weight in the BMP2-treated PE model group (Fig. 6b–g), without affecting plasma sFlt-1 levels, urine albumin/creatinine ratio and glomeruli damage in both non-model group and the vehicle-treated PE model group (Fig. S5a–c).

A previous study has demonstrated that a decrease in systolic blood pressure by 10 mmHg was associated with a reduced risk of preeclampsia and eclampsia in humans (OR per 10 mmHg reduction in SBP 0.57, 95% CI 0.53–0.60, $P = 1.11 \times 10^{-84}$).[69] In addition, for every 10 mmHg decrease in diastolic blood pressure, the level of cardiovascular risk is reduced by 50% in humans.[70] In our study, BMP2 supplementation led to a blood pressure reduction of 10.3 mmHg (95% CI:5.3–15.0) and a diastolic blood pressure of 15.0 mmHg (95% CI:12.3–18.3) in rats, suggesting that BMP2 could have a clinically significant role in preventing and treating preeclampsia, in addition to its statistical significance.

Notably, significantly increased placental *Bmp2* mRNA levels were observed in the Ad Flt1-induced PE rat model (Fig. S5d), which is consistent with the finding of increased placental BMP2 levels during late gestation in PE patients. To examine the potential physiological changes of BMP2 treatment in rats during pregnancy, we measured the body weight and bone morphogenesis of pregnant rats with or without recombinant BMP2 supplementation. The body weight of pregnant rats did not show significant differences on G7 and G19 between the PBS and BMP2 groups (Fig. S5e). In addition, the bone morphogenesis at various positions (including the head, neck, thorax, abdomen, hip, pelvic, and spine) was examined by micro-CT, and the results show that recombinant BMP2 treatment (10 μg/kg/day from G10–G13 days) did not influence bone formation of pregnant rats (Fig. S5f). Taken together, these *in vivo* experimental findings support the supplementation of recombinant BMP2 acts as a useful intervention to treat PE-related phenotypes.

Discussion

Numerous studies have examined various strategies for alleviating PE[71,72]; however, this disease remains challenging to manage in the clinic owing to its poorly understood pathophysiology. The leading hypotheses strongly rely on observations of insufficient trophoblast invasion during early pregnancy, which is understood as one of the initiating events during PE pathogenesis.[3] Our results uncover an axis between Hofbauer cells and trophoblasts mediated by BMP2-BMPR1A signalling that can compensate for shallow trophoblast invasion in preeclamptic placentas (Fig. 7), which supports a complex model for PE pathogenesis and could facilitate the development of effective diagnostic and therapeutic strategies for PE management.

TGF-β superfamily members have been shown to exert divergent functions in regulating trophoblast invasion and have been proposed as diagnostic and therapeutic candidates for PE.[8] Consistent with the inhibitory effects of TGF-β1-3 and Nodal on trophoblast invasion, increased expression levels of these molecules have been observed in PE patients.[73,74] Meanwhile, activin A, a well-defined pro-invasive factor in trophoblasts,[75–77] has also been detected to be upregulated in the third trimester of preeclamptic pregnancies. Similar to activin A, leptin is another pro-invasive factor in human trophoblasts and has been found to be upregulated in PE patients.[78] Both activin A and leptin are used as circulating biomarkers for PE.[79] While these findings may, at first, appear contradictory, it should be

pretreated with vehicle (DMSO), ACVR1 and BMPR1A inhibitor DMH-1 (1 μM), or ACVR1B, TGFβRI and ACVR1C inhibitor SB431542 (10 μM) for 60 min followed by treatment with or without BMP2 (25 ng/mL) for 1 h (upper panel) or 48 h (lower panel). The protein levels of targets were assayed by immunoblotting. **c-d**, HTR8/SVneo cells were transfected with 20 nM non-targeting control siRNA or siRNA targeting *ACVR1B* and *TGFBR1* (**c**) or *ACVR1* and *BMPR1A* (**d**) for 48 h prior to treatment with or without BMP2 (25 ng/mL) for 1 h (upper panel) or 48 h (lower panel). The protein levels of targets were assayed by immunoblotting. **e**, **g** and **h**, Two published single cell transcriptomes of placentas from 5 preeclamptic donors and 5 healthy donors were integrated and re-analyzed. **e**, t-SNE plot (left panel) and violin plot (right panel) displays the *BMPR1A* expression level in all cell types. **g**, Violin plot displays the expression level of PE related DEGs in $BMPR1A^{+}$ VCTs and $BMPR1A^{-}$ VCTs. **h**, Dot plots displays the significantly enriched gene sets using the DEGs in **g**. Dot size represents the number of DEGs from a particular gene set (count). **f**, Immunofluorescence staining of E-cadherin and BMPR1A in first-trimester placental villi. The lower panel is higher powered images of the upper panel. VCT, villous cytotrophoblast; SCT, syncytiotrophoblast; CCC, cytotrophoblast cell column. Scale bar, 40 μm.

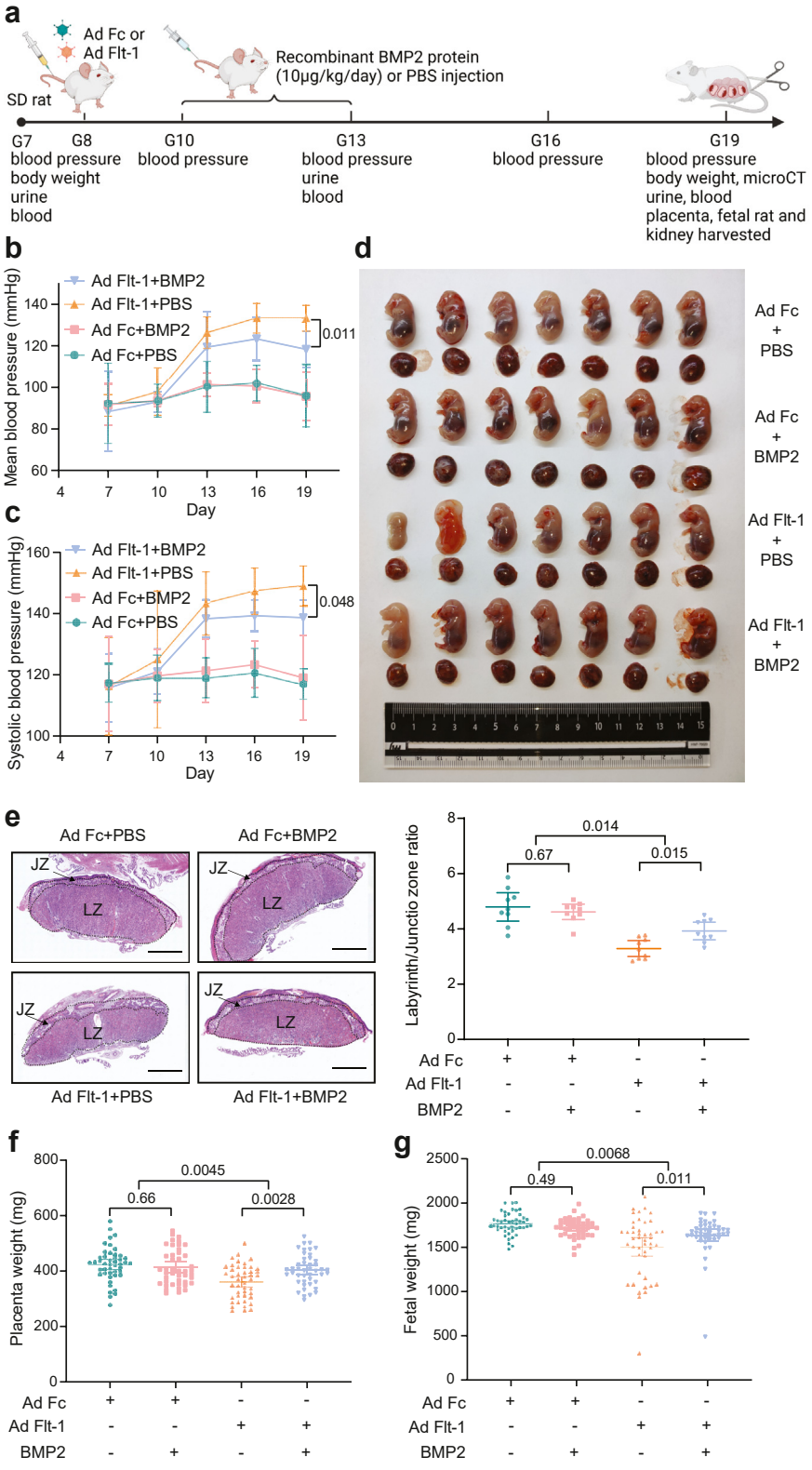

***Fig. 6:* Supplementation with recombinant BMP2 alleviates PE-related phenotypes in Ad Flt1-induced PE rat model**. a, Diagram illustrates the animal experimental protocol. Adenoviruses expressing sFlt-1 or control Fc were injected into the tail vein of Sprague–Dawley rats on G8.

noted that the upregulation of placental BMP2 was observed in the late-gestational age of pregnancy, when a compensatory effect could have manifested and become detectable. Although this kind of compensatory mechanism has not been reported in PE, previous studies have reported that certain upregulated biomarkers could be therapeutic drugs (as recombinant protein) for hypertensive diseases; for example, natriuretic peptide, a biomarker of hypertrophic cardiomyopathy and high blood pressure, can confer anti-hypertrophic and blood-pressure lowering effects.[80,81] Thus, the increased levels of pro-invasive factors such as activin A, leptin, BMP2, and BMP6 in late gestational period of PE may—beyond being circulating biomarkers for PE occurrence—function in a compensatory response to shallow trophoblast invasion during early PE pathogenesis.

We observed the enrichment of BMP2 in Hofbauer cells at the maternal–fetal interface, with the expression levels even higher in placentas from PE patients compared to healthy pregnancies. Notably, we observed increased BMP6 levels in the serum obtained on the morning of the day of delivery in PE patients compared to healthy pregnancies; however, BMP2 levels were barely detectable in these serum samples. The increased BMP2 levels were detected in placentas in late gestation. Considering the pro-angiogenic roles of BMPs,[11] these findings suggest that the effects of BMP2 are local to the placenta, while those of BMP6 could be systemic, including its effects on maternal endothelium in addition to the placenta. As placental villous macrophages of fetal origin, Hofbauer cells resemble M2-like phenotype, functioning in placental morphogenesis and homeostasis.[52] Further investigations regarding paracrine regulatory roles of Hofbauer cells on different cell types at the maternal–fetal interface could better elucidate the potential therapeutic application of cytokines and growth factors derived from Hofbauer cells in preeclampsia.

Controversies exist regarding the dysregulation direction of BMP2 in preeclamptic placentas since a recent study has revealed that decreased BMP2 expression in the placenta may contribute to the onset of severe preeclampsia.[82] However, we would like to point out that consistent with our multi-omics analyses, the placental transcriptomes from other bulk RNAseq and scRNA-seq databases also show increased *BMP2* in preeclamptic placentas.[28,29,47] This inconsistent finding regarding either decreased (by Yi et al.)[82] or increased placentas BMP2 expression levels in preeclampsia could be due to the different locations/gestational ages of placental samples collected by different groups; we consistently collected the central area of full-term placenta adjacent to the maternal side and the placentas examined with RNA-seq in our study were from patients at higher gestational age (33.05 weeks for PE vs. 37.61 weeks for HP) as compared to the patients of Yi's study (29–30 weeks).[82] Moreover, Yi's study analyzed microarray and RNA-seq datasets from patients with early-onset PE, which accounts for 5–20% of all PE cases, while our study included samples from both early-onset and late-onset PE patients (mostly late-onset PE patients). These distinctions can potentially help explain the differences in the findings about placental BMP2 levels in PE patients. Notably, our data show that placental *BMP2* mRNA levels were negatively correlated with the severity of PE, supporting the essential role of BMP2 signalling in preventing PE progression, which reach a consensus with the above mentioned study that insufficient BMP2 signalling at the maternal fetal-interface leads to preeclampsia occurrence and progression.[82]

Even though the upregulated placental BMP2 and circulating BMP6 levels were detected at the end of pregnancy, it is not clear if such changes occur during the early stages of human placental development (i.e., the first 4 months of pregnancy, when greater invasion and remodeling occur). Studies examining the early gestational age of pregnancy are difficult to conduct in PE research; however, we measured first-trimester maternal serum of PE patients and healthy pregnancies (34 vs. 34 individuals) from the human biobank of our large-scale assisted reproductive cohort platform: maternal circulating BMP2 and BMP6 levels in the first trimester of pregnancy were both below the detection range. Notably, we observed significantly increased *Bmp2* mRNA levels in the Ad Flt1-induced PE rat model, which is consistent with the finding of increased placental BMP2 levels during late gestation in PE patients. The current data suggest that the BMP2 signaling enhancement regulated by H3K27me3 and the

The pregnant rats then were subjected to tail vein recombinant BMP2 protein (10 μg/kg) or PBS injection daily from G10 to G13. Rats from 4 groups including Ad Fc + PBS (n = 3), Ad Fc + BMP2 (n = 3), Ad Flt1 + PBS (n = 3), and Ad Flt1 + BMP2 (n = 3) were harvested on G19 with fetal rats and tissues collection. Blood pressure was measured and recorded every three days from G7 to G19. Urine and blood samples were collected on G7, G13 and G19. **b-c**, Mean blood pressure (MBP) and systolic blood pressure (SBP) of pregnant rats from each group (n = 3) were analyzed. **d**, The representative image of fetal rats and placentas (G19) from each group (n = 7). **e**, HE staining of rat placentas was performed to observe placental labyrinth and junction areas. Representative images were presented in left panel and the placental labyrinth/junction ratios in each group were quantified and summarized in right panel (n = 9). Scale bar, 2 mm. **f-g**, The weight of fetal rats and corresponding placentas was determined on G19 in Ad Fc + PBS group (n = 46), Ad Fc + BMP2 group (n = 44), Ad Flt1 + PBS group (n = 45) and Ad Flt1 + BMP2 group (n = 44). Quantitative results are expressed as the mean with 95% CI and p values by two-way ANOVA are labeled.

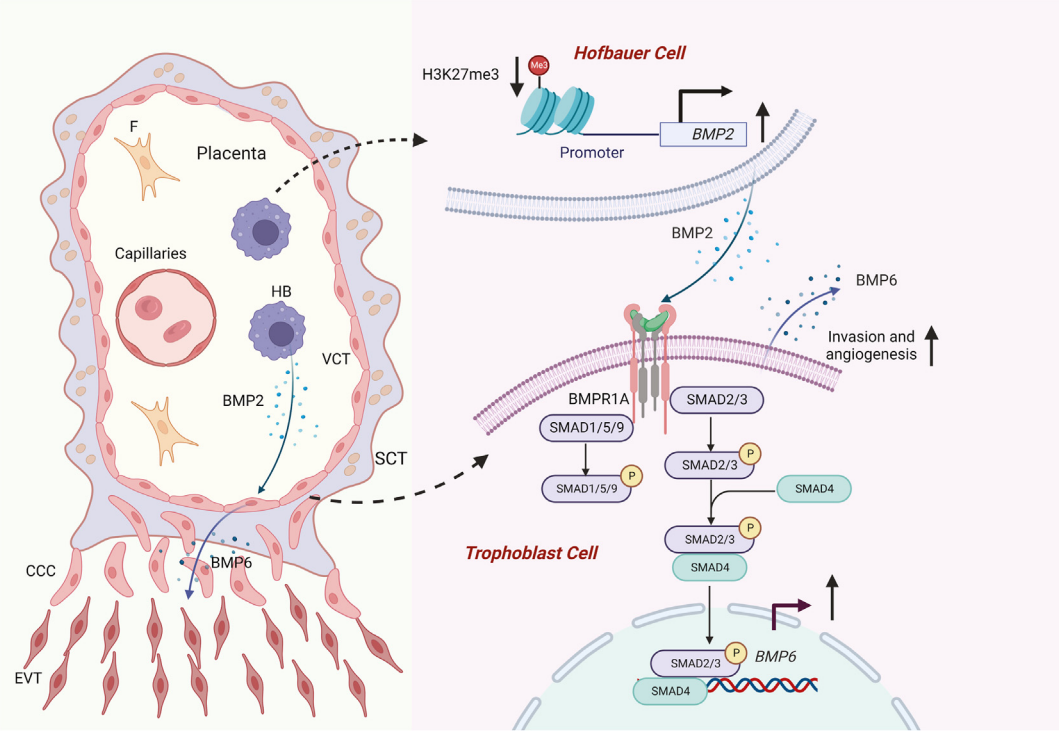

Fig. 7: **H3K27me3-modulated Hofbauer cell BMP2 signalling enhancement compensates for shallow trophoblast invasion in pre-eclampsia**. By taking advantage of clinical samples from healthy and preeclamptic pregnant participants, as well as *in vitro*, *ex vivo* and *in vivo* experimental models, we found that BMP2, a pro-invasive factor of human trophoblast, was upregulated in preeclamptic placentas with Hofbauer cells as its cellular origin; Reduced H3K27me3 modification contributes to the observed BMP2 upregulation in preeclamptic placentas; BMP6, a downstream target of BMP2 and a newly identified pro-invasive factor in trophoblasts, was upregulated in late gestational serum of patients with preeclampsia; BMP2 promotes trophoblast invasion and vascular mimicry by upregulating BMP6 expression in a BMPR1A-SMAD2/3-SMAD4-dependent manner. Our findings demonstrate that epigenetically regulated Hofbauer cell-derived BMP2 signalling enhancement in late gestation could serve as a compensatory response for shallow trophoblast invasion in PE, suggesting opportunities for diagnostic marker and therapeutic target applications in PE clinical management. This schematic diagram is created with Biorender.com.

elevated circulating BMP6 levels at late gestational age could be a late compensatory consequence of the placental developmental dysfunction that occurred in the early gestational stage of PE patients, rather than its cause.

Our findings show that BMP6 is a human trophoblast pro-invasive factor and mediates the pro-invasive impacts of elevated BMP2 levels. Moreover, we demonstrate that, whereas BMP2 activates both canonical SMAD1/5/9 and non-canonical SMAD2/3 signalling, only SMAD2/3 signalling is required for its upregulation of BMP6. BMP6 has been suggested as a candidate marker for predicting cardiovascular disease.[83] Moreover, recombinant BMP6 has been approved for clinical application to accelerate bone healing.[84] BMP6's current use as a disease biomarker and its commercial availability as a protein drug lend support to the idea of potentially exploiting BMP6 for the diagnosis of PE and perhaps even as a therapeutic intervention. Given the established roles of BMPs in angiogenesis,[11] it is conceivable that the increased placental BMP2 levels (and subsequent increase in circulating BMP6 levels) protect against the pathogenesis of PE by both increasing trophoblast invasion and impairing endothelial dysfunction.

By utilizing a PE-like rat model induced by Ad Flt1 injection, we found significantly alleviated PE-like phenotypes after recombinant BMP2 supplementation. Since the elevated sFlt-1, which is an antiangiogenic factor and induced by Ad Flt1 injection, could lead to PE-related phenotypes,[85] the protective effects observed after BMP2 supplementation could be attributed to the altered expression of proangiogenic factors, including placental-secreted placental growth factor (PlGF) and BMP6, which are BMP2's downstream molecules. Even though, we observed alleviated insufficient placental development in Ad Flt1-induced PE rats after recombinant BMP2 supplementation, supporting this intervention as a useful measure to treat PE-related poor placentation. Considering the known pro-angiogenic

roles of BMPs, the beneficial effect of BMP2 supplementation in alleviating PE-related phenotypes in PE-like rats could be explained by its pro-invasive effects on trophoblasts in early pregnancy or by its impacts on maternal tissues such as repairing endothelial dysfunction. In addition, although our study demonstrated a positive association between high placental BMP2 levels during late gestation and the occurrence of PE, it does not necessarily contradict the protective roles played by BMP2 in placental development previously demonstrated by functional studies using animal models. It is conceivable that the upregulation of BMP2 detected in the third trimester of pregnancy could represent a compensatory response to the shallow trophoblast invasion that occurs in the first trimester of pregnancy. Admittedly, detailed *in vivo* mechanisms and strategies for alleviating PE worth further investigation, especially with the advancement of animal models which could better recapitulate PE pathophysiology.

As a FDA-approved drug for bone graft substitutes, BMP2 (usually used at the concentration of 1.5 mg/mL in humans for inducing consistent bone formation) has also been reported to have many side-effects, including ectopic bone formation, osteoclast-mediated bone resorption, and inappropriate adipogenesis.[86] To determine the effects of BMP2 supplementation during pregnancy, we examined the maternal body weight and bone formation in pregnant rats given a dose of 10 μg/kg/day. This dosage effectively alleviated symptoms in a rat model of Ad Flt1-induced PE without changing maternal body weight or bone formation. However, further investigation is necessary to fully understand the potential side effects of BMP2 supplementation during pregnancy.

Our study suggests a compensatory role of H3K27me3-modulated human Hofbauer cell BMP2 signalling for shallow trophoblast invasion in PE. However, potential uncontrolled confounders, including maternal age, BMI, and pre-existing medical conditions, could influence both H3K27me3 and BMP2 signalling and thus may have affected our results. Furthermore, we acknowledge that the experimental models used in our study, while useful, may not fully recapitulate the complex *in vivo* conditions. Therefore, further validation, ideally through prospective research in a larger and diverse cohort, is warranted to substantiate our findings.

The relatively small number of clinical samples is a limitation of our study. Perspective studies are also needed to further evaluate the diagnostic value of BMP6 with different combinations of other biomarkers in PE. Although we found increased BMP6 levels in sera from PE patients, we did not observe significantly increased *BMP6* mRNA levels in preeclamptic placentas compared to healthy placentas, possibly owing to the high abundance of *BMP6* transcription in human placentas and the secretory nature of the BMP6 protein. The difficulty in collecting gestational age-matched placentas from fully healthy pregnant women with large sample sizes is a perennial challenge in PE studies; PE is frequently accompanied by iatrogenic preterm birth, and the majority of spontaneous preterm labor without PE is associated with inflammation. Consistent with a previous study,[87] our results show comparable levels of H3K27me3 in the second and third trimesters of healthy placentas, thus excluding the possibility of artificial observations due to the relatively smaller gestational age of preeclamptic placentas compared to healthy placentas.

In conclusion, our findings uncover an epigenetic-regulated trophoblast BMP2 signalling enhancement in preeclamptic placentas that compensates for shallow trophoblast invasion during PE pathogenesis. We also identify BMP6 as a pro-invasive factor in human trophoblasts and a circulating biomarker for PE occurrence. Studies of molecules and signalling pathways for compensating for or alleviating shallow trophoblast invasion, particularly in the context of PE pathogenesis, warrant further attention and seem likely to promote efforts to develop drug-based interventions for the diagnosis and treatment of PE caused by insufficient trophoblast invasion. That is, the identification of molecules and pathways that can repair placental dysfunction could provide valuable diagnostic and/or therapeutic targets for PE clinical management, which could reduce the considerable burden of morbidity, mortality, and long-term cardiovascular disease risk associated with PE.

Contributors

Y.L. and W.W. conceived and designed the study; JY.D., HJ.Z., CP.H., XY.W. and XX.L. performed experiments; Y.L., W.W., and JY.D. analyzed data; Y.Z., HJ.Z. performed bioinformatics analysis, and W.W. supervised the analysis; JL.M. and CL.W. collected clinical tissue and serum samples; JY.D. and W.W. verified the underlying data; Y.L., W.W., JY.D., HJ.Z., and Y.Z. wrote the manuscript; Z-J.C. and J.H.Y. critically revised the manuscript. All authors have been involved in interpreting the data and approved the final version.

Data sharing statement

The original RNA-seq and ChIP-seq data for this study have been deposited at the Genome Sequence Archive for Human (GSA-Human, https://ngdc.cncb.ac.cn/gsa-human) with the accession numbers HRA001421 and HRA001422. Qualified researchers may apply for access to original data pending institutional review board approval. This study did not generate new unique reagents, and all materials are available commercially, as shown in Supplementary Table S1. Further information and requests for resources and reagents should be directed to and will be fulfilled by Yan Li (yanli.sdu@gmail.com).

Declaration of interests

We declare that none of the authors have any conflicts of interest with the content of this manuscript.

Acknowledgments

This work was supported by grants from the National Key Research and Development Program of China (2022YFC2702400), the National Natural Science Foundation of China (82101784, 82171648, 31988101), and the Natural Science Foundation of Shandong Province (ZR2020QH051, ZR2020MH039).

Appendix A. Supplementary data

Supplementary data related to this article can be found at https://doi.org/10.1016/j.ebiom.2023.104664.

References

1 Hogan MC, Foreman KJ, Naghavi M, et al. Maternal mortality for 181 countries, 1980-2008: a systematic analysis of progress towards Millennium Development Goal 5. *Lancet*. 2010;375(9726):1609–1623.
2 Steegers EA, von Dadelszen P, Duvekot JJ, Pijnenborg R. Pre-eclampsia. *Lancet*. 2010;376(9741):631–644.
3 Rana S, Lemoine E, Granger JP, Karumanchi SA. Preeclampsia: pathophysiology, challenges, and perspectives. *Circ Res*. 2019;124(7):1094–1112.
4 Tooher J, Thornton C, Makris A, Ogle R, Korda A, Hennessy A. All hypertensive disorders of pregnancy increase the risk of future cardiovascular disease. *Hypertension*. 2017;70(4):798–803.
5 Staff AC. The two-stage placental model of preeclampsia: an update. *J Reprod Immunol*. 2019;134–135:1–10.
6 Redman C. The six stages of pre-eclampsia. *Pregnancy Hypertens*. 2014;4(3):246.
7 Redman CW, Sargent IL. Latest advances in understanding pre-eclampsia. *Science*. 2005;308(5728):1592–1594.
8 Li Y, Yan J, Chang HM, Chen ZJ, Leung PCK. Roles of TGF-beta superfamily proteins in extravillous trophoblast invasion. *Trends Endocrinol Metab*. 2021;32(3):170–189.
9 Katagiri T, Watabe T. Bone morphogenetic proteins. *Cold Spring Harb Perspect Biol*. 2016;8(6).
10 Monsivais D, Nagashima T, Prunskaite-Hyyrylainen R, et al. Endometrial receptivity and implantation require uterine BMP signaling through an ACVR2A-SMAD1/SMAD5 axis. *Nat Commun*. 2021;12(1):3386.
11 Dyer LA, Pi X, Patterson C. The role of BMPs in endothelial cell function and dysfunction. *Trends Endocrinol Metab*. 2014;25(9):472–480.
12 Zhao HJ, Klausen C, Li Y, Zhu H, Wang YL, Leung PCK. Bone morphogenetic protein 2 promotes human trophoblast cell invasion by upregulating N-cadherin via non-canonical SMAD2/3 signaling. *Cell Death Dis*. 2018;9(2):174.
13 Xu RH, Chen X, Li DS, et al. BMP4 initiates human embryonic stem cell differentiation to trophoblast. *Nat Biotechnol*. 2002;20(12):1261–1264.
14 Valera E, Isaacs MJ, Kawakami Y, Izpisua Belmonte JC, Choe S. BMP-2/6 heterodimer is more effective than BMP-2 or BMP-6 homodimers as inductor of differentiation of human embryonic stem cells. *PLoS One*. 2010;5(6):e11167.
15 Lichtner B, Knaus P, Lehrach H, Adjaye J. BMP10 as a potent inducer of trophoblast differentiation in human embryonic and induced pluripotent stem cells. *Biomaterials*. 2013;34(38):9789–9802.
16 Kohan-Ghadr HR, Kadam L, Jain C, Armant DR, Drewlo S. Potential role of epigenetic mechanisms in regulation of trophoblast differentiation, migration, and invasion in the human placenta. *Cell Adhes Migrat*. 2016;10(1–2):126–135.
17 Ashraf UM, Hall DL, Rawls AZ, Alexander BT. Epigenetic processes during preeclampsia and effects on fetal development and chronic health. *Clin Sci (Lond)*. 2021;135(19):2307–2327.
18 Apicella C, Ruano CSM, Mehats C, Miralles F, Vaiman D. The role of epigenetics in placental development and the etiology of preeclampsia. *Int J Mol Sci*. 2019;20(11).
19 Margueron R, Reinberg D. The Polycomb complex PRC2 and its mark in life. *Nature*. 2011;469(7330):343–349.
20 Rahat B, Sharma R, Bagga R, Hamid A, Kaur J. Imbalance between matrix metalloproteinases and their tissue inhibitors in pre-eclampsia and gestational trophoblastic diseases. *Reproduction*. 2016;152(1):11–22.
21 Sanulli S, Justin N, Teissandier A, et al. Jarid2 methylation via the PRC2 complex regulates H3K27me3 deposition during cell differentiation. *Mol Cell*. 2015;57(5):769–783.
22 Kaneda A, Fujita T, Anai M, et al. Activation of Bmp2-Smad1 signal and its regulation by coordinated alteration of H3K27 trimethylation in Ras-induced senescence. *PLoS Genet*. 2011;7(11):e1002359.
23 Practice ACoO. ACOG practice bulletin. Diagnosis and management of preeclampsia and eclampsia. Number 33, January 2002. American College of Obstetricians and Gynecologists. *Int J Gynaecol Obstet*. 2002;77(1):67–75.
24 Hypertension in pregnancy. Report of the American College of obstetricians and gynecologists' task force on hypertension in pregnancy. *Obstet Gynecol*. 2013;122(5):1122–1131.
25 Maynard SE, Min J-Y, Merchan J, et al. Excess placental soluble fms-like tyrosine kinase 1 (sFlt1) may contribute to endothelial dysfunction, hypertension, and proteinuria in preeclampsia. *J Clin Investig*. 2003;111(5):649–658.
26 Kuo CJ, Farnebo F, Yu EY, et al. Comparative evaluation of the antitumor activity of antiangiogenic proteins delivered by gene transfer. *Proc Natl Acad Sci U S A*. 2001;98(8):4605–4610.
27 Wang W, Cohen JA, Wallrapp A, et al. Age-related dopaminergic innervation augments T helper 2-type allergic inflammation in the postnatal lung. *Immunity*. 2019;51(6):1102–1118.e7.
28 Zhou W, Wang H, Yang Y, Guo F, Yu B, Su Z. Trophoblast cell subtypes and dysfunction in the placenta of individuals with pre-eclampsia revealed by SingleCell RNA sequencing. *Mol Cell*. 2022;45(5):317–328.
29 Zhang T, Bian Q, Chen Y, et al. Dissecting human trophoblast cell transcriptional heterogeneity in preeclampsia using single-cell RNA sequencing. *Mol Genet Genom Med*. 2021;9(8):e1730.
30 Thomas JR, Appios A, Zhao X, et al. Phenotypic and functional characterization of first-trimester human placental macrophages, Hofbauer cells. *J Exp Med*. 2021;218(1).
31 Charan J, Kantharia ND. How to calculate sample size in animal studies? *J Pharmacol Pharmacother*. 2013;4(4):303–306.
32 Love MI, Huber W, Anders S. Moderated estimation of fold change and dispersion for RNA-seq data with DESeq2. *Genome biology*. 2014;15(12):550.
33 Satija R, Farrell JA, Gennert D, Schier AF, Regev A. Spatial reconstruction of single-cell gene expression data. *Nat Biotechnol*. 2015;33(5):495–502.
34 Enquobahrie DA, Meller M, Rice K, Psaty BM, Siscovick DS, Williams MA. Differential placental gene expression in pre-eclampsia. *Am J Obstet Gynecol*. 2008;199(5):566.e1–566.e11.
35 Tan KH, Tan SS, Sze SK, Lee WK, Ng MJ, Lim SK. Plasma biomarker discovery in preeclampsia using a novel differential isolation technology for circulating extracellular vesicles. *Am J Obstet Gynecol*. 2014;211(4):380.e1–380.e13.
36 Wang Y, Lim R, Nie G. HtrA4 may play a major role in inhibiting endothelial repair in pregnancy complication preeclampsia. *Sci Rep*. 2019;9(1):2728.
37 Mootha VK, Lindgren CM, Eriksson KF, et al. PGC-1alpha-responsive genes involved in oxidative phosphorylation are coordinately downregulated in human diabetes. *Nat Genet*. 2003;34(3):267–273.
38 Subramanian A, Tamayo P, Mootha VK, et al. Gene set enrichment analysis: a knowledge-based approach for interpreting genome-wide expression profiles. *Proc Natl Acad Sci U S A*. 2005;102(43):15545–15550.
39 Vitoratos N, Economou E, Iavazzo C, Panoulis K, Creatsas G. Maternal serum levels of TNF-alpha and IL-6 long after delivery in preeclamptic and normotensive pregnant women. *Mediat Inflamm*. 2010;2010:908649.
40 Shamshirsaz AA, Paidas M, Krikun G. Preeclampsia, hypoxia, thrombosis, and inflammation. *J Pregnancy*. 2012;2012:374047.
41 Lee KY, Jeong JW, Wang J, et al. Bmp2 is critical for the murine uterine decidual response. *Mol Cell Biol*. 2007;27(15):5468–5478.
42 Acevedo LG, Bieda M, Green R, Farnham PJ. Analysis of the mechanisms mediating tumor-specific changes in gene expression in human liver tumors. *Cancer Res*. 2008;68(8):2641–2651.
43 Heller G, Schmidt WM, Ziegler B, et al. Genome-wide transcriptional response to 5-aza-2'-deoxycytidine and trichostatin a in multiple myeloma cells. *Cancer Res*. 2008;68(1):44–54.
44 Lu C, Han HD, Mangala LS, et al. Regulation of tumor angiogenesis by EZH2. *Cancer Cell*. 2010;18(2):185–197.
45 Meissner A, Mikkelsen TS, Gu H, et al. Genome-scale DNA methylation maps of pluripotent and differentiated cells. *Nature*. 2008;454(7205):766–770.
46 Nuytten M, Beke L, Van Eynde A, et al. The transcriptional repressor NIPP1 is an essential player in EZH2-mediated gene silencing. *Oncogene*. 2008;27(10):1449–1460.
47 Ren Z, Gao Y, Gao Y, et al. Distinct placental molecular processes associated with early-onset and late-onset preeclampsia. *Theranostics*. 2021;11(10):5028–5044.
48 Ukah UV, Hutcheon JA, Payne B, et al. Placental growth factor as a prognostic tool in women with hypertensive disorders of pregnancy: a systematic review. *Hypertension*. 2017;70(6):1228–1237.

49 Zhao HJ, Klausen C, Zhu H, Chang HM, Li Y, Leung PCK. Bone morphogenetic protein 2 promotes human trophoblast cell invasion and endothelial-like tube formation through ID1-mediated upregulation of IGF binding protein-3. *FASEB J*. 2020;34(2):3151–3164.
50 Zhao HJ, Chang HM, Zhu H, Klausen C, Li Y, Leung PCK. Bone morphogenetic protein 2 promotes human trophoblast cell invasion by inducing activin A production. *Endocrinology*. 2018;159(7):2815–2825.
51 Vento-Tormo R, Efremova M, Botting RA, et al. Single-cell reconstruction of the early maternal-fetal interface in humans. *Nature*. 2018;563(7731):347–353.
52 Reyes L, Golos TG. Hofbauer cells: their role in healthy and complicated pregnancy. *Front Immunol*. 2018;9:2628.
53 Tumes DJ, Onodera A, Suzuki A, et al. The polycomb protein Ezh2 regulates differentiation and plasticity of CD4(+) T helper type 1 and type 2 cells. *Immunity*. 2013;39(5):819–832.
54 You J, Wang W, Chang HM, et al. The BMP2 signaling Axis promotes invasive differentiation of human trophoblasts. *Front Cell Dev Biol*. 2021;9:607332.
55 Chau K, Hennessy A, Makris A. Placental growth factor and pre-eclampsia. *J Hum Hypertens*. 2017;31(12):782–786.
56 Knofler M, Pollheimer J. Human placental trophoblast invasion and differentiation: a particular focus on Wnt signaling. *Front Genet*. 2013;4:190.
57 Mack JJ, Iruela-Arispe ML. NOTCH regulation of the endothelial cell phenotype. *Curr Opin Hematol*. 2018;25(3):212–218.
58 van Nieuw Amerongen GP, Koolwijk P, Versteilen A, van Hinsbergh VW. Involvement of RhoA/Rho kinase signaling in VEGF-induced endothelial cell migration and angiogenesis in vitro. *Arterioscler Thromb Vasc Biol*. 2003;23(2):211–217.
59 Leung KW, Cheung LW, Pon YL, et al. Ginsenoside Rb1 inhibits tube-like structure formation of endothelial cells by regulating pigment epithelium-derived factor through the oestrogen beta receptor. *Br J Pharmacol*. 2007;152(2):207–215.
60 Sokol ES, Feng YX, Jin DX, et al. SMARCE1 is required for the invasive progression of in situ cancers. *Proc Natl Acad Sci U S A*. 2017;114(16):4153–4158.
61 Chang HM, Qiao J, Leung PC. Oocyte-somatic cell interactions in the human ovary-novel role of bone morphogenetic proteins and growth differentiation factors. *Hum Reprod Update*. 2016;23(1):1–18.
62 Hao J, Ho JN, Lewis JA, et al. In vivo structure-activity relationship study of dorsomorphin analogues identifies selective VEGF and BMP inhibitors. *ACS Chem Biol*. 2010;5(2):245–253.
63 Inman GJ, Nicolas FJ, Callahan JF, et al. SB-431542 is a potent and specific inhibitor of transforming growth factor-beta superfamily type I activin receptor-like kinase (ALK) receptors ALK4, ALK5, and ALK7. *Mol Pharmacol*. 2002;62(1):65–74.
64 Cruickshank T, MacDonald TM, Walker SP, et al. Circulating growth differentiation factor 15 is increased preceding preeclampsia diagnosis: implications as a disease biomarker. *J Am Heart Assoc*. 2021;10(16):e020302.
65 Guo Y, Gao Y, Liu S. lncRNA XIST is associated with preeclampsia and mediates trophoblast cell invasion via miR-340-5p/KCNJ16 signaling pathway. *Transpl Immunol*. 2022;74:101666.
66 Hastie R, Brownfoot FC, Pritchard N, et al. EGFR (epidermal growth factor receptor) signaling and the mitochondria regulate sFlt-1 (soluble FMS-like tyrosine kinase-1) secretion. *Hypertension*. 2019;73(3):659–670.
67 Karumanchi SA, Stillman IE. In vivo rat model of preeclampsia. *Methods Mol Med*. 2006;122:393–399.
68 Li Z, Zhang Y, Ying Ma J, et al. Recombinant vascular endothelial growth factor 121 attenuates hypertension and improves kidney damage in a rat model of preeclampsia. *Hypertension*. 2007;50(4):686–692.
69 Ardissino M, Slob EAW, Rajasundaram S, et al. Safety of beta-blocker and calcium channel blocker antihypertensive drugs in pregnancy: a Mendelian randomization study. *BMC Med*. 2022;20(1):288.
70 Law MR, Morris JK, Wald NJ. Use of blood pressure lowering drugs in the prevention of cardiovascular disease: meta-analysis of 147 randomised trials in the context of expectations from prospective epidemiological studies. *BMJ*. 2009;338:b1665.
71 Bergmann A, Ahmad S, Cudmore M, et al. Reduction of circulating soluble Flt-1 alleviates preeclampsia-like symptoms in a mouse model. *J Cell Mol Med*. 2010;14(6B):1857–1867.
72 Li ZH, Wang LL, Liu H, et al. Galectin-9 alleviates LPS-induced preeclampsia-like impairment in rats via switching decidual macrophage polarization to M2 subtype. *Front Immunol*. 2018;9:3142.
73 Nadeem L, Munir S, Fu G, et al. Nodal signals through activin receptor-like kinase 7 to inhibit trophoblast migration and invasion: implication in the pathogenesis of preeclampsia. *Am J Pathol*. 2011;178(3):1177–1189.
74 Caniggia I, Grisaru-Gravnosky S, Kuliszewsky M, Post M, Lye SJ. Inhibition of TGF-beta 3 restores the invasive capability of extravillous trophoblasts in preeclamptic pregnancies. *J Clin Invest*. 1999;103(12):1641–1650.
75 Caniggia I, Lye SJ, Cross JC. Activin is a local regulator of human cytotrophoblast cell differentiation. *Endocrinology*. 1997;138(9):3976–3986.
76 Li Y, Klausen C, Cheng JC, Zhu H, Leung PC. Activin A, B, and AB increase human trophoblast cell invasion by up-regulating N-cadherin. *J Clin Endocrinol Metab*. 2014;99(11):E2216–E2225.
77 Li Y, Zhu H, Klausen C, Peng B, Leung PC. Vascular endothelial growth factor-A (VEGF-A) mediates activin A-induced human trophoblast endothelial-like tube formation. *Endocrinology*. 2015;156(11):4257–4268.
78 Taylor BD, Ness RB, Olsen J, et al. Serum leptin measured in early pregnancy is higher in women with preeclampsia compared with normotensive pregnant women. *Hypertension*. 2015;65(3):594–599.
79 Bersinger NA, Smarason AK, Muttukrishna S, Groome NP, Redman CW. Women with preeclampsia have increased serum levels of pregnancy-associated plasma protein A (PAPP-A), inhibin A, activin A and soluble E-selectin. *Hypertens Pregnancy*. 2003;22(1):45–55.
80 Woods RL. Cardioprotective functions of atrial natriuretic peptide and B-type natriuretic peptide: a brief review. *Clin Exp Pharmacol Physiol*. 2004;31(11):791–794.
81 van der Velde AR, Meijers WC, de Boer RA. Biomarkers for risk prediction in acute decompensated heart failure. *Curr Heart Fail Rep*. 2014;11(3):246–259.
82 Yi Y, Zhu H, Klausen C, et al. Dysregulated BMP2 in the placenta may contribute to early-onset preeclampsia by regulating human trophoblast expression of extracellular matrix and adhesion molecules. *Front Cell Dev Biol*. 2021;9:768669.
83 Ong KL, Chung RWS, Hui N, et al. Usefulness of certain protein biomarkers for prediction of coronary heart disease. *Am J Cardiol*. 2020;125(4):542–548.
84 Mizrahi O, Sheyn D, Tawackoli W, et al. BMP-6 is more efficient in bone formation than BMP-2 when overexpressed in mesenchymal stem cells. *Gene Ther*. 2013;20(4):370–377.
85 Fan X, Rai A, Kambham N, et al. Endometrial VEGF induces placental sFLT1 and leads to pregnancy complications. *J Clin Invest*. 2014;124(11):4941–4952.
86 James AW, LaChaud G, Shen J, et al. A review of the clinical side effects of bone morphogenetic protein-2. Tissue engineering Part B. *Reviews*. 2016;22(4):284–297.
87 Zhang B, Kim MY, Elliot G, et al. Human placental cytotrophoblast epigenome dynamics over gestation and alterations in placental disease. *Dev Cell*. 2021;56(9):1238–12352.e5.